HIV-1 Envelope glycoprotein modulates CXCR4 clustering and dynamics on the T cell membrane

Adriana Quijada-Freire[1], César A. Santiago[2], Eva M. García-Cuesta[1], Blanca Soler-Palacios[1], Rosa Ayala-Bueno[1], Sofía R. Gardeta[1], Enara San Sebastian[3], Eva Armendariz-Burgoa[4], María C. Puertas[4], Ricardo Villares[1], Urtzi Garaigorta[3], Luis Ignacio González-Granado[5,6], José Miguel Rodríguez-Frade[1], Jakub Chojnacki[4,7,8], Javier Martinez-Picado[4,7,9,10], Mario Mellado[1*]

[1]Chemokine Signaling group, Department of Immunology and Oncology, Centro Nacional de Biotecnología/CSIC, Campus de Cantoblanco, 28049, Madrid, Spain

[2]X-ray Crystallography Unit, Department of Macromolecules Structure, Centro Nacional de Biotecnología/CSIC, Campus de Cantoblanco, 28049, Madrid, Spain

[3]Departamento de Biología Molecular y Celular, Centro Nacional de Biotecnología/CSIC Campus de Cantoblanco, 28049, Madrid, Spain.

[4]IrsiCaixa, 08916, Badalona, Spain.

[5]12 de Octubre Health Research Institute (imas12), E-28012 Madrid, Spain.

[6]Department of Public Health School of Medicine, School of Medicine Universidad Complutense de Madrid, E-28040 Madrid, Spain.

[7]CIBERINFEC, 28029, Madrid, Spain

[8]Germans Trias i Pujol Research Institute (IGTP), 08916, Badalona, Spain

[9]University of Vic-Central University of Catalonia, 08500, Vic, Spain

[10]Catalan Institution for Research and Advanced Studies (ICREA), 08010 Barcelona, Spain.

[*]Corresponding author: Mario Mellado, Department of Immunology and Oncology, CNB/CSIC, Darwin 3, Cantoblanco, 28049 Madrid Spain. Tel: (+34) 91/585-4852; Fax: (+34) 91/372-0493; e-mail: mmellado@cnb.csic.es

Abstract

HIV-1 entry into susceptible cells requires the dynamic interaction of its envelope (Env) glycoprotein with the host cell receptor CD4 and a co-receptor, either CCR5 or CXCR4. While the core molecular mechanisms driving Env-receptor interactions and subsequent membrane fusion are well characterized, the precise nanoscale spatial reorganization of these co-receptors at the viral binding site remains poorly defined. In this study, we employed single-particle tracking total internal reflection fluorescence (SPT-TIRF) microscopy to quantitatively analyze nanoscale organizational changes of CXCR4 on the surface of $CD4^+$ T cells following binding by X4-tropic HIV-1. Our data reveal that both recombinant X4-gp120 and virus-like particles expressing physiological levels of X4 Env proteins (gp120 and gp41) promote CXCR4 clustering, a phenomenon linked to cell infection. Furthermore, these ligands induced oligomerization of $CXCR4^{R334X}$, a naturally occurring mutant associated with WHIM syndrome that supports HIV-1 infection but fails to oligomerize in response to CXCL12. Our findings establish a link between CXCR4 clustering and HIV-1 infection, enhancing our understanding of the initial events in viral attachment and entry. These results further suggest that HIV-1 depends on a specific spatial arrangement of co-receptors, distinct from that induced by their natural chemokine ligands, highlighting the critical role of cell-surface receptor spatial organization in dictating cellular function.

Introduction

HIV-1 infects immune cells through a dynamic interaction between its envelope glycoprotein complex (Env), composed of gp41 and gp120 trimers (1, 2), and two receptors on target cells: the primary receptor CD4, and a co-receptor, either CCR5 or CXCR4. These co-receptors are critical for viral entry and determine viral tropism. R5 strains (M-tropic) infect primary macrophages and certain memory $CD4^+$ T cells by binding to CD4 and CCR5(3), while X4 strains (T-tropic) infect primary $CD4^+$ T cells by binding to CD4 and CXCR4 (4).

R5-tropic viruses are typically the primary mode of transmission in humans and remain prevalent throughout the infection (5). However, in many infected individuals, the virus evolves its tropism over time, progressing from R5-tropic to dual-tropic (R5/X4), and ultimately to X4-tropic as the infection advances (6). This shift in tropism is associated with a more rapid decline in $CD4^+$ T cell counts (7). Furthermore, CXCR4 has been implicated in the infection of hematopoietic progenitor cells, potentially contributing to the establishment of long-lasting latent HIV-1 reservoirs (8).

The fusion of viral and cellular membranes is initiated by the binding of gp120 to CD4 (9, 10), which triggers a conformational change in gp120 that facilitates co-receptor engagement (11). These structural changes expose the N-terminal hydrophobic fusion peptide of gp41, which inserts into the cell membrane (12) to establish a fusion pore and release the viral contents into the target cell.

Numerous structural and biophysical studies have examined the HIV-1 infection process, successfully clarifying the structural requirements and conformational changes in gp120 and gp41 that enable membrane fusion and viral entry (13–16). Early investigations into host cell components revealed that HIV-1 infection induces the redistribution of cell-surface CD4 and co-receptors to the sites of viral attachment (17,

18). More recent evidence, obtained through super-resolution microscopy, demonstrates that HIV-1 binding triggers CD4 clustering, a phenomenon also observed (albeit to a lesser degree) following stimulation with gp120 alone (19). However, less is known about which specific co-receptors are also recruited to the virus particles bound to the cell surface. It is known that gp120 can mediate the association of CD4 with both CXCR4 and CCR5 (17, 20, 21). Furthermore, it has been shown that the co-expression of CCR5 modifies the conformation of both CXCR4 homodimers and CD4/CXCR4 heterodimers. This conformational change prevents the binding of gp120 from an X4 HIV-1 strain, specifically $gp120_{IIIB}$, to the resulting CD4/CXCR4/CCR5 complex (22).

Large-scale molecular assemblies at the cell membrane, often termed signaling clusters or nanoclusters, are increasingly recognized as key regulators of cell signaling (23). Evidence indicates that the spatial reorganization and distribution of membrane receptors are key to controlling cell functions. Notably, clustering also appears to be essential for viral infection. For instance, Env–CD4 complexes form clusters and ring-like structures, facilitating closer contact between opposing membranes (24). These clusters often govern a significant portion of the overall signaling process and are frequently associated with the cytoskeleton (23). For example, CD4 receptors exist in pre-clustered structures that enlarge upon T cell activation, thereby modulating the strength of the signaling response (25, 26). Moreover, CXCR4 is organized at the cell membrane as monomers, dimers and small aggregates (groups of ≥3 receptors) called nanoclusters. The binding of its specific ligand, CXCL12, leads to a decrease in the proportion of monomers/dimers, while simultaneously increasing the formation of larger nanoclusters. This change in receptor organization consequently alters the lateral mobility of CXCR4 within the cell membrane (27). This mechanism is critical for initiating CXCR4 signaling and enabling cells to accurately orient themselves in response to CXCL12 gradients (28).

A naturally occurring CXCR4 mutant, $CXCR4^{R334X}$, which is responsible for WHIM syndrome, a severe immunological disorder (29), fails to form these large nanoclusters upon CXCL12 binding. Consequently, cells carrying this mutation lose their ability to properly sense chemoattractant gradients (28).

Here, we employed quantitative single-particle tracking in total internal reflection fluorescence (SPT-TIRF) microscopy to directly investigate the spatial arrangement and dynamic activity of CXCR4 upon exposure to HIV-1 glycoproteins. Our findings reveal that both recombinant X4-gp120 and virus-like particles (VLPs) containing a limited number of X4 Env proteins (gp120 and gp41) promote CXCR4 clustering on cells expressing CD4 and CXCR4. Moreover, they trigger the oligomerization of $CXCR4^{R334X}$. These results suggest that, along with CD4 clustering, the conformational changes in chemokine receptors triggered by HIV-1 are essential for cell infection and differ from the effects of the natural ligand, CXCL12. Therefore, CD4/CXCR4 complexes and their interaction sites represent potentially valuable targets for developing novel therapeutic strategies to block HIV-1 entry.

Materials and methods

Cells and reagents

HEK-293T cells, Jurkat human leukemia cells ($JKCD4^{-}X4^{+}$), and Daudi cells were obtained from the American Type Culture Collection (CRL-3216, CRL-10915 and CCL- 213, respectively; ATCC, Rockville, MD). HEK-293CD4 cells, Jurkat $CD4^{+}$ cells ($JKCD4^{+}X4^{+}$), and Jurkat cells expressing an X4-tropic HIV-1 Env (JKHXBC2) were kindly provided by Drs. G. del Real (Instituto Nacional de Investigación y Tecnología Agraria y Alimentaria, Madrid, Spain) and J. Alcamí (Centro Nacional de Microbiología, Instituto de Salud Carlos III, Madrid, Spain). Where indicated, Jurkat cells lacking endogenous *CXCR4* ($JKCD4^{+}X4^{-}$) (30) were electroporated with plasmids expressing wild-type CXCR4-AcGFP or mutant $CXCR4^{R334X}$-AcGFP receptors (20 μg), as described (30). Stable Jurkat cells expressing $CXCR4^{R334X}$ ($JKCD4^{+}CXCR4^{R334X}$) were generated by electroporation with $CXCR4^{R334X}$ and antibiotic selection (30).

Human peripheral blood mononuclear cells (PBMCs) were isolated from the blood of a patient with WHIM syndrome ($CXCR4^{R334X}$) or from healthy donors, and when required from buffy coats of healthy donors, which were obtained from the Centro de Transfusiones (Comunidad Autónoma de Madrid, Spain) by centrifugation through Percoll density gradients (760 × g, 45 min, room temperature [RT]). $CD4^{+}$ cells were purified by negative selection using Dynabeads (Invitrogen, Thermo Fisher Scientific, Waltham, MA) and activated *in vitro* for 1 week with 50 U/mL of IL-2 (Teceleukin; Roche, Nutley, NJ) and 5 μg/mL phytohemagglutinin (Roche, Basel, Switzerland) to generate T cell blasts (31). The study using blood from WHIM patients and healthy donors was approved by the Institutional Review Board of the 12 de Octubre Health Research Institute (Nº CEIm: 24/248), and was conducted according to the principles of the Declaration of Helsinki. Informed consent was obtained from all patients.

Recombinant gp120 protein, HXBc2, was obtained from MyBiosource (#MBS43404, MyBiosource Inc., San Diego, CA). The following antibodies were used: anti-human CXCR4 monoclonal antibody (mAb) (clone 44717) and phycoerythrin-conjugated anti-human CXCR4 mAb (clone 12G5; both from R&D Systems, Minneapolis, MN); goat F(ab')2 anti-mouse IgG-PE (Southern Biotech, Birmingham, AL); anti-human CD4 mAb (clone OKT4; Biolegend, San Diego, CA); anti-histidine mAb (clone AD1.1.10; R&D Systems); rabbit anti-gp120$_{IIIb}$ Ab (32); rabbit anti-Gag p24 HIV-1 mAb (R&D Systems); and anti-phospho-AKT mAb (S473; #4060), anti-phospho-ERK1,2 mAb (T202/Y204; #9191), and anti-phospho-Lck mAb (Y505; #2751) (all from Cell Signaling Technology, Danvers, MA); anti-tubulin mAb conjugated with rhodamine (Bio-Rad, Hercules, CA); phalloidin-TRITC (#P1951, Sigma-Merck, St Louis, MO); anti-ICAM 3 mAb (clone HP2/19) kindly donated by Dr. Francisco Sánchez Madrid (Instituto Sanitario Hospital Universitario La Princesa); goat anti-mouse-AF488 Ab (Thermo Fisher Scientific); anti-human gp120 mAb Fab fragments (clone 2G12; Polymun Scientific, Vienna, Austria); anti-human IgG Fab fragments (Jackson ImmunoResearch, West Grove, PA) conjugated to Abberior STAR RED (Abberior GmbH, Gottingen, Germany), kindly donated by Dr. Jakub Chojnacki (Germans Trias i Pujol Research Institute (IGTP)); anti-p24 HIV-1 (clone 37G12; Polymun Scientific) conjugated with Abberior STAR ORANGE. Human CXCL12 was obtained from PeproTech (Rocky Hill, NJ), and human CXCR4 was cloned into the pAcGFPm-N1 plasmid (Clontech Laboratories, Palo Alto, CA), as described (33).

Fab fragments for staining in stimulated emission depletion (STED) microscopy were generated from the respective IgGs using the Fab Micro Preparation 3 Kit (Pierce, Thermo Fisher Scientific). The quality of Fab preparations was determined by measuring the absorbance of the eluted fractions of each conjugated antibody (at 280 nm and at the

wavelength of maximum absorption of the fluorochrome). Anti-human Fab fragments were coupled to Abberior STAR RED dye *via* NHS-ester chemistry according to the dye manufacturer's instructions.

CellTracker Orange CMTMR and Blue CMAC (#C2927 and #C2110, respectively) were from Thermo Fisher Scientific.

Gene constructs

Genes of HIV-1 gp120 (residues 31-507) from the isolate HXB2 (HIV-1_{IIIB}), with a C-terminal 6×histidine tag, were amplified by PCR from pHXB2-env (#1069 NIH-AIDS Reagent Program) using the oligonucleotides 5'NheI (5' TAACCGGTGCCAC CATGGACAGAGCCAAGCTGCTGCTGTTGCTGCTGCTGCTGCTGCTGCCTCAG GCTCAGGCCACTGAGAAGCTGTGGGTG 3') and 3'NotI (5' ATGCGGCCGCTCA GTGATGGTGATGGTGATGGGATCCACGCGGAACCAGCTGCACCACTCTTCT 3'), and were cloned into pIRES-PURO3 (#631619 from Clontech Laboratories).

The CD4 extracellular domain (residues 1-388), with a C-terminal 6×histidine tag, was amplified by PCR from CD4-pcDNA-3.1, kindly donated by Dr. Santos Mañes (Centro Nacional de Biotecnología, CSIC) (34) using the oligonucleotides 5'AgeI (5' TAACCGGTATGAACCGGGGAGTCCCT 3') and 3' NotI (5' ATGCGGCCGCCTAGTATG GTGATGGTGATGCAAGTCCTCTTCAGAAATGAGCTTTTGCTCGGGCAGAACCT TGAT 3'), and was cloned into pIRES-PURO3 (#631619 from Clontech Laboratories). Stably-transfected HEK-293T cell lines were generated for each construct. Briefly, 0.5 × 10^6 cells were seeded in DMEM supplemented with 10% FCS in a 6-well plate 24 hours before transfection. Cells were then transfected with Expifectamine in OptiMem media (ExpiFectamine™ 293 transfection kit; #A14525 from Thermo Fisher Scientific). At 48 hours post-transfection, cells were transferred to DMEM containing 10% FBS and 2 μg/mL puromycin for selection (1 × 10^4 cells per well in a 96-well plate). Protein expression was confirmed by western blotting (using anti-gp120IIIB or anti-histidine

mAbs, depending on the construct). Positive clones were expanded, frozen, and stored in liquid nitrogen.

Purification of recombinant proteins: soluble HIV-1 gp120 and soluble CD4

HEK-293T cells expressing C-terminal his-tagged HXB2-gp120 or the extracellular CD4 domain were grown in DMEM containing 10% FBS and 2 μg/mL puromycin in 150-mm plates. The filtered supernatants were passed through a Nickel Agarose Extrachel column, Ni-NTA, (ABT technologies, Madrid, Spain) at a flow rate of 0.5 mL/min. Each recombinant histidine-tagged protein was eluted utilizing a step-gradient protocol using a Tris 50 mM pH 8, NaCl 500 mM buffer containing 500 mM imidazole. The elution involved initial steps of 10% and 20% imidazole, followed by a linear gradient to 100% to ensure complete protein recovery. The eluted fractions were analyzed by SDS-PAGE gel electrophoresis. Those fractions containing the protein of interest were pooled and concentrated to a final volume of 0.5 mL. The concentrated sample was subjected to gel filtration chromatography using a S200 Increase (10/300) column (Cytiva, Freiburg, Germany). The eluted fractions were analyzed by SDS-PAGE and fractions containing the expected molecular size were pooled, aliquoted, and stored at -80ºC.

Production of viral-like particles and lentiviral particles

Production of VLPs in HEK-293T cells included transfection with a plasmid encoding the X4-tropic HIV-1 Env (10 μg pHXB2env; #1069 NIH-AIDS Reagent Program) and a plasmid encoding a second-generation packaging system (7 μg psPAX2; #12260 Addgene, Watertown, MA). Supernatants were collected 48 hours post-transfection, filtered through 0.45 μm filters, and clarified by ultracentrifugation (247,000 × g, 2 h, 4°C) on a 20% sucrose cushion, using a Beckman SW55 rotor. The resulting VLPs were aliquoted and stored at -80°C. Expression of gp120 and p24 was assessed by western

blotting with specific antibodies. Each VLP batch was quantified using a p24 Quantikine ELISA kit (R&D Systems).

Production of lentiviral particles (LVPs) was performed as above with the co-transfection of a reporter gene (8 μg plGFP; #PS100065, OriGene, Rockville, MD) instead of the double transfection. Supernatants were collected 48 hours post-transfection, filtered through 0.45 μm filters, aliquoted, and stored at -80°C. Expression of gp120 and p24 was assessed by western blotting with specific antibodies. Each LVP batch was characterized in a transduction assay using LVPs transfected with the vesicular stomatitis virus G glycoprotein (VSVG) (pCMV-VSV-G; #8454, Addgene) as a positive control.

Western blotting

Cells (3×10^6) were activated with CXCL12 (50 nM) or recombinant X4-gp120 (0.3 μg/mL) at the time points indicated and then lysed in RIPA detergent buffer containing 1 mM PMSF, 10 μg/mL aprotinin, 10 μg/mL leupeptin, and 10 μM sodium orthovanadate (30 min, 4ºC). Cell extracts were analyzed by western blotting using specific antibodies. Densitometric evaluation of western blots was performed using ImageJ software (NIH, Bethesda, MD).

Flow cytometry

Cells (2×10^5/well) were incubated with specific antibodies (30 min, 4ºC) and mean fluorescence intensity (MFI) was determined on a Gallios or FC500 flow cytometer (Beckman Coulter). When required, Jurkat cells expressing CD4 ($JKCD4^+X4^+$ and $JKCD4^+X4^-$) were incubated with X4-gp120-His (0.3 μg/mL), followed by staining with an anti-histidine-PE mAb. Similarly, Daudi cells were incubated with a mixture of X4-gp120 (0.3 μg/ml) and soluble hCD4-his (0.2 μg/mL), and subsequently stained with an anti-histidine-PE mAb.

For human PBMCs, 100 μL of whole blood from healthy controls and a WHIM patient were analyzed by flow cytometry for the expression of CD3-APC (IM2467), CD19-PC5.5 (A66328), CD4-FITC (A07750), CD8-PC7 (737661; all from Beckman Coulter Inc., Brea, CA), and CXCR4-PE (306506, Biolegend) using a Gallios flow cytometer and FlowJo software.

Receptor internalization was evaluated after cell activation (5×10^5 cells/well) with 50 nM CXCL12 or 0.3 μg/mL of recombinant X4-gp120 at the indicated time points. Cells were incubated with an anti-CXCR4 mAb (clone 44717, 30 min, 4°C), followed by a PE-coupled goat anti-mouse IgG (30 min, 4ºC) or, when required, with anti-CD4 (clone OKT4, 20 min, 4ºC), and analyzed in a Cytoflex cytometer (Beckman Coulter). Results are expressed as a percentage of mean spot intensity (MSI) of treated cells relative to that of unstimulated cells.

To evaluate VLPs by flow cytometry, particles were coupled to latex beads (4 mm, 4% w/v Aldehyde/Sulfate latex; Invitrogen, Eugene, OR). After sonication (5 min, RT), beads were mixed with VLPs at a ratio of 1:1 v/v (15 min, RT) in 1% casein-PBS solution (Bio-Rad). Reactive groups were blocked with 100 mM glycine (60 min, 4°C, with continuous rocking). Beads coupled to VLPs were washed twice by centrifugation (3 min, 2000 × g) in washing buffer (PBS/BSA 0.5%), resuspended, and incubated with the corresponding dilution of the recombinant soluble CD4 in casein-PBS solution (30 min, RT). VLP-beads conjugates were washed three times (3 min, 2,000 × g) with PBS staining buffer (PBS supplemented with 2% FBS, 1% BSA, and 0.2% sodium azide) and stained as above for flow cytometry.

Lentiviral particle transduction assays

HEK-293 CD4 cells (1.2×10^4 cells per well in a 96-well plate) were inoculated with serial dilutions of LVP-containing supernatants. Stock solutions were diluted in DMEM,

10% FCS, 1 mM pyruvate, and 2 mM glutamine. Sixteen hours later, the viral inoculum was replaced with fresh medium and the cells were further incubated (48 h, 37°C). Viral transduction efficiency was determined by GFP fluorescence analysis. The medium was discarded and cells were washed with PBS and fixed using 4% formaldehyde in PBS (20 min, RT). Fluorescence was imaged in a Tecan Spark Cyto plate reader (Tecan Group Ltd., Männedorf, Switzerland) after extensive washes with PBS. Images of 2456 × 2052 pixels at a 16-bit gray scale were acquired with a 4× objective. All images were captured using identical exposure settings (200 ms), except for wells where cells were transduced with LVPs expressing VSVG, for which an exposure time of 80 ms was used. Mean fluorescence intensity of GFP signal of each image was quantitated using Fiji/ImageJ v2.3.0/1.53t software.

Cell-cell fusion assay

The JKHXBC2 cell line was co-cultured with the indicated Jurkat target cells at a 1:1 ratio in 96-well flat-bottom plates (16 h, 37°C). Prior to co-culture, each cell type was stained with vital probes CellTracker Orange CMTMR and Blue CMAC, respectively. Double-stained events were subsequently analyzed using a Gallios Analyzer cytometer (Beckman Coulter). Results are shown as the percentage of fusion events ± SD, using as a reference the fusions events detected in JKCD4$^+$CXCR4$^+$ cells.

Cell adhesion/migration on planar lipid bilayers

Planar lipid bilayers were prepared as reported (35). Briefly, unlabeled GPI-linked intercellular adhesion molecule 1 (ICAM-1) liposomes were mixed with 1,2-dioleoyl-phosphatidylcoline. Membranes were assembled in FCS2 chambers (Bioptechs, Butler, PA), blocked with PBS containing 2% FCS (60 min, RT), and coated with CXCL12 (200 nM, 30 min, RT) or gp120 (0.3 μg/ml, 30 min, RT). Cells (3×10^6 CD4$^+$ T blasts/mL) in PBS containing 0.5% FCS, 0.5 g/L D-glucose, 2 mM $MgCl_2$, and 0.5 mM $CaCl_2$ were

then injected into the pre-warmed chamber (37ºC). Confocal fluorescence, differential interference contrast (DIC) and interference reflection microscopy (IRM) images were acquired on a Zeiss Axiovert LSM 510-META inverted microscope with a 40× oil-immersion objective. Imaris 7.0 software (Bitplane, Zurich, Switzerland) and ImageJ 1.49v were used for qualitative and quantitative analysis of cell dynamics parameters, fluorescence and IRM signals. The fluorescence signal of the planar bilayer in each case was established as the background fluorescence intensity. The frequency of adhesion (IRM^+ cells) per image field was estimated as [nº of cells showing IRM contact/total number of cells (estimated by DIC)] × 100; similarly, we calculated the frequency

STED assays

Purified particles (~1 μg of p24) were adhered to glass cover slips previously coated with 0.01% poly-L-lysine (Sigma) for 20 minutes. Cover slips were briefly fixed with 3% PFA/PBS and blocked using 2% BSA (Sigma)/PBS for 30 minutes. Particles were stained for Env using 10 ng/μL 2G12 Fab fragments and anti-human Abberior STAR RED-conjugated Fab fragments. Following immunostaining, particles were washed in permeabilization buffer (0.1% saponin, 0.5% BSA in PBS) and stained for Gag using 20 ng/μL 37G12 Ab conjugated with STAR ORANGE. The samples were briefly fixed using 3% PFA/PBS again and were overlaid with SlowFade Diamond (Thermo Fisher Scientific). All steps were carried out at RT.

The VLPs were imaged using an Olympus IX83 inverted confocal microscope equipped with the Abberior STEDYCON STED system using a 60×/1.42NA objective. The following parameters were used during STED image acquisitions: pinhole size: 1 Airy; dwell time: 300 μs/pixel; field of view: 20 μm × 20 μm and pixel size: 20 nm.

The mature state of VLPs, the percentage which express gp120 on their surface and the intensity of the signal of gp120 per VLP, were quantified manually using ImageJ.

Imaging of viral-like particles by transmission electron microscopy

The integrity of VLPs was examined by negative-stain electron microscopy on carbon grids. Samples were incubated on the grids and were treated with 2% uranyl acetate (30 s, RT). Grids were examined using a transmission electron microscope (1200-EX II; Jeol, Tokyo, Japan) at 100 kV, equipped with a Gatan Oneview CMOS camera.

FRET saturation curves by sensitized emission

FRET analyses were performed as described (36). Briefly, HEK-293T cells (3.5×10^5 cells/well) were transiently transfected with cDNA encoding the fusion proteins using the poly-ethylenimine method (Sigma-Aldrich). For CD4/CXCR4 or CD4/CXCR4^{R334X} heterodimers, the cells were co-transfected with a fixed amount of CD4-CFP (2 μg) and increasing amounts of CXCR4-YFP or CXCR4^{R334X}-YFP (0.5–8.0 μg). As a control, we used a fixed amount of CD4-CFP (2 μg) and increasing amounts of 5HT$_{2B}$-YFP (0.5–12 μg). We incubated cells with cDNA and poly-ethylenimine (5.47 mM in nitrogen residues) and 150 mM NaCl in serum-free medium, which was replaced after 4 hours by complete medium. At 48 hours post transfection, cells were washed twice in HBSS supplemented with 0.1% glucose and resuspended in the same solution. Total protein concentration was determined for whole cells using the Bradford Assay Kit (Bio-Rad). Cell suspensions (0.2 μg/μL) were added to black 96-well microplates and emission light was quantified using the Wallac Envision 2104 Multilabel Reader (Perkin-Elmer, Waltham, MA) as described (27). To determine FRET$_{50}$ and FRET$_{max}$ values, curves were extrapolated from data using a nonlinear regression equation applied to a single binding site model with a 95% confidence interval (GraphPad PRISM software, San Diego, CA). When FRET at a fixed ratio was needed, HEK-293T cells were transiently co-transfected with a fixed ratio of CXCR4-YFP/CD4-CFP (15 μg and 9 μg, respectively) and CXCR4^{R334X}-YFP/CD4-CFP (9 μg and 9 μg, respectively in all cases). After 48 hours the

cells were treated with Env(-) VLPs (0.1 μg/mL of Gag p24) or gp120-VLPs (0.1 μg/mL of Gag p24) and FRET efficiency was evaluated (n = 3, mean ± SD).

Single-molecule TIRF imaging and analysis

Transfected cells expressing 8,500–22,000 receptors/cell (<4.5 particles/μm^2) were selected for detection and tracking analysis. Experiments were performed at 37ºC with 5% CO_2 using a TIRF microscope (Leica AM TIRF inverted microscope; Leica Microsystems, Wetzlar, Germany). Image sequences of individual particles (500 frames) were then acquired at 49% laser power (488-nm diode laser) with a frame rate of 10 Hz (100 ms/frame). The penetration depth of the evanescent field was 90 nm. Particles were detected and tracked using the U-Track2 algorithm (37) implemented in MATLAB, as described (27). MSI, number of mobile and immobile particles and diffusion coefficients (D_{1-4}) were calculated from the analysis of thousands of single trajectories over multiple cells (statistics provided in the respective figure captions) using described routines (27). The receptor number along individual trajectories was determined as reported (38), using the intensity of the monomeric protein CD86-AcGFP as a reference (Supplementary Figure 1). Values were confirmed using single-step photobleaching analysis (27, 28).

HIV-1 infection in T CD4$^+$ cells of a WHIM patient

All donors were female and under the age of 30. PBMCs were obtained from sero-negative fresh blood of a WHIM patient and three healthy donor controls using SepMate tubes (STEMCELL Technologies, Vancouver, Canada). Isolated PBMCs were cultured in RPMI supplemented with 20% FBS (Gibco), 1% penicillin/streptomycin (Capricorn Scientific GmbH, Ebsdorfergrund, Germany), 3 μg/mL PHA (Sigma-Aldrich), and 10 U/mL of IL-2 (Novartis, Basel, Switzerland) for 48 hours at 37°C. Activated PBMCs were inoculated *in vitro* at a multiplicity of infection (MOI) of 0.001 with the HIV-1 NL4-3 lab strain for 1 hour. After removal of the viral inoculum, cultures were split into two

wells and maintained in RPMI supplemented with 20% FBS, 1% penicillin/streptomycin, and 10 U/mL of IL-2. Supernatants were collected at different time points and replaced with fresh supplemented media. The infection rate was determined by quantification of viral p24 in the supernatants using the Alliance HIV-1 p24 Antigen Elisa Kit (Perkin Elmer).

Statistical analyses

All results were analyzed with GraphPad Prism software version 9. Cell polarization assays, using immunofluorescence or planar lipid bilayers comparing different conditions, were analyzed to determine significant differences between means using one-way analysis of variance (ANOVA) followed by Tukey's multiple comparisons test. Data related to the percentage of mature VLPs and their surface expression of gp120 obtained by STED microscopy, and MFI results by flow cytometry, were also analyzed by one-way ANOVA and Tukey's multiple comparisons test. A two-tailed Mann-Whitney non-parametric test was used to analyze the MFI of gp120 per VLP. The Kruskal-Wallis test followed by Dunn's test was used to analyze MSI and diffusion coefficients (D_{1-4}) of single particles in TIRF experiments. We used contingency tables to compare two or more groups of categorical variables, such as the percentages of mobile or immobile particles, and these were compared using a Chi-square test with a two-tailed p-value. Statistical differences were reported as n.s. = not significant $p > 0.05$, $*p \leq 0.05$, $**p \leq 0.01$, $***p \leq 0.001$ and $****p \leq 0.0001$.

Results

Recombinant gp120-mediated CXCR4 clustering requires CD4 expression

To evaluate the role of HIV-1 in modulating CXCR4 dynamics at the cell membrane, we first synthesized a recombinant X4 HIV-1 gp120 (X4-gp120) with a C-terminal histidine tag to facilitate subsequent detection. We generated a HEK-293T cell line that constitutively secretes the recombinant glycoprotein. The secreted X4-gp120 was isolated from cell culture supernatants using a simple, rapid, non-denaturing and efficient purification procedure involving Ni-NTA agarose chromatography and gel filtration chromatography. The purity of the isolated glycoprotein was confirmed by SDS-PAGE and western blotting, using commercial gp120 as a control and specific antibodies (Supplementary Figure 2A, B). The X4-gp120 specifically bound to Jurkat cells expressing CD4, regardless of the presence or absence of CXCR4 (JKCD4^{+}CXCR4^{+} and JKCD4^{+}CXCR4^{-}, respectively) (Supplementary Figure 2C). By contrast, X4-gp120 did not bind to Daudi cells, which express only CXCR4 (Supplementary Figure 2D). In this latter case, X4-gp120 binding became possible when the recombinant protein was pre-incubated with soluble CD4. As a control, no binding of soluble CD4 was detected in the absence of X4-gp120 (Supplementary Figure 2D). These data indicate that our recombinant gp120 is a X4-tropic gp120 capable of binding Jurkat cells expressing CD4.

Engagement of the HIV-1 Env with CD4 and/or a chemokine co-receptor activates several signal transduction pathways (39, 40). For instance, gp120 binding to CD4 leads to the phosphorylation of the receptor tyrosine kinase p56Lck, which then activates the Raf/MEK/ERK and phosphatidylinositol 3-kinase (PI3K) pathways (41). PI3K is also activated through chemokine receptor engagement (42), and only viruses capable of inducing signaling *via* these receptors can establish productive infections (40). Jurkat cells and primary CD4^{+} T blasts were stimulated with X4-gp120, then lysed and analyzed

by western blotting. The results showed that Akt, ERK1/2 and Lck were rapidly phosphorylated following X4-gp120 activation (Supplementary Figure 3A, B) in both cell types. Furthermore, it is known that the interaction of gp120 with CXCR4 influences the actin cytoskeleton (43). Cytochalasin D, an inhibitor of F-actin polymerization, has been shown to inhibit viral entry into PBMCs (44), and to affect the formation of HIV-1 reverse transcriptase products in HeLa cells (45). We thus evaluated whether X4-gp120 reorganized the actin cytoskeleton of the target cells. Using artificial lipid bilayers coated with ICAM-1, we observed that both CXCL12 and X4-gp120 induced the polarization of primary $CD4^+$ T blasts and, furthermore, enhanced cell adhesion (Supplementary Figure 4A, B). However, only CXCL12 triggered significant cell migration (Supplementary Figure 4C). These findings confirmed that X4-gp120 bound CXCR4 in the presence of CD4 and was fully functional on both primary $CD4^+$ T blasts and Jurkat cells.

The actin cytoskeleton acts as a physical barrier, influencing the compartmentalization of the plasma membrane and the dynamics of membrane proteins (46, 47). Consequently, the dynamic nature of actin not only defines cell shape during migration, but also affects membrane organization of both CD4 (48) and CXCR4 (27). Next, we transiently transfected $JKCD4^+X4^-$ cells, which express endogenous CD4, with CXCR4-AcGFP. We then used SPT in TIRF-M mode to observe individual molecules within the plasma membrane, allowing us to determine the effect of X4-gp120 on CXCR4 dynamics and stoichiometry (Supplementary video 1-3). Consistent with previous observations (27, 28), our analysis of CXCR4 dynamics in unstimulated cells revealed that the majority of CXCR4 particles were mobile (~87%) (Figure 1A), exhibiting a median short time-lag diffusion coefficient ($D_{1–4}$) of 0.017 $\mu m^2 s^{-1}$ (Figure 1B). Upon stimulation, both CXCL12 and X4-gp120 significantly reduced the overall receptor diffusivity (CXCL12, median $D_{1–4}$ = 0.007 $\mu m^2\ s^{-1}$; X4-gp120, median $D_{1–4}$ = 0.009 μm^2

s^{-1}) (Figure 1B), and increased the percentage of immobile particles from ~13% (basal) to ~20% (CXCL12), and to ~18% (X4-gp120) (Figure 1A). Mobile particles exhibited distinct diffusion profiles, derived from mean square displacement (MSD) plots (49), and were further classified based on motion using the moment scaling spectrum (50). For most mobile particles (~90% in unstimulated cells, ~79% in CXCL12-activated cells, and ~75% in X4-gp120 stimulated cells), diffusion was confined (Supplementary Figure 5A). To quantify the number of receptors in individual trajectories, we measured the average fluorescence intensity during the initial 20 frames of each trajectory and used the intensity of the monomeric protein CD86-AcGFP as a reference (28, 51) (Supplementary Figure 1). In unstimulated cells, we found a predominance of CXCR4 monomers and dimers (~98%), with only a minor fraction of oligomers, complexes containing more than three receptors (~2%). Upon the addition of saturating X4-gp120 concentrations, we observed a significant reduction in the percentage of monomers and dimers (~82%) and a corresponding increase in nanoclusters composed of ≥3 receptors/particle (~18%) (Figure 1C). This observation aligns with previous findings for CXCL12 (27) As a control, stimulation with CXCL12 resulted in a larger percentage of these nanoclusters (~26%) (Figure 1C). These data correlated with the higher MSI values observed after cell activation (basal 933 a.u.; CXCL12 2,105 a.u., X4-gp120 1,738 a.u.) (Figure 1D). Collectively, these results indicate that X4-gp120 triggers CXCR4 nanoclustering, although to a lesser extent than CXCL12.

gp120-expressing virus-like particles mediate CXCR4 clustering

Recombinant X4-gp120 alone does not fully replicate the function of HIV-1 Env. Previous studies have shown that the Env consists of gp120 trimers that redistribute and cluster on the surface of virions following proteolytic Gag cleavage during maturation (52). Considering the low number of Env trimers on natural HIV virions (53–55), this

clustering is crucial for establishing multiple receptor interactions necessary for virus entry. To mimic the behavior of the virus, we prepared VLPs containing the X4 HIV-1 Env. HEK-293T cells were transiently transfected with pHXB2env, psPAX2, and, when required, a pLentiGFP plasmid that encodes a GFP reporter gene flanked by LTR regions. In this latter case, we generated LVPs because these budding particles contained genetic material and could transduce target cells. Supernatants were collected 48-hours post transfection, and VLPs were purified by ultracentrifugation and resuspended in PBS. The structural integrity of the VLPs was confirmed using negative-stain electron microscopy (Supplementary Figure 6A). Western blot analysis of the samples, culture media, and clarified supernatants confirmed the presence of both gp120 and p24 in VLPs and LVPs (Supplementary Figure 6B). The gp120-containing viral particles bound soluble CD4 (Supplementary Figure 6C) and the corresponding LVPs successfully infected HEK-293CD4 cells, as demonstrated in transduction assays (Supplementary Figure 6D, E). LVPs containing VSVG were utilized as a positive control in these functional assays (Supplementary Figure 6D, E).

Immature HIV-1 particles exhibit reduced entry efficiency (56, 57). This effect may stem from the rigidity of the immature Gag lattice beneath the viral membrane, which hinders membrane fusion (58) interactions between Gag and Env glycoproteins, limiting the lateral mobility of the sparsely distributed Env trimers and, consequently, impairing the clustering necessary for efficient infection (13). Therefore, we evaluated the maturation status of the generated VLPs using STED microscopy. We compared the condensation of Gag and the distribution of Env molecules on the surface of the VLPs with those observed on genetically immature particles and integrase-defective NL4-3ΔIN virions, serving as controls (13). Env proteins were stained with the human mAb 2G12, which specifically recognizes the gp120 domain. To avoid antibody-induced clustering,

we used purified Fab fragments of 2G12. The location of individual HIV-1 particles was determined using the human mAb 37G12, which targets the Gag protein and served as a "counterstain" reference (Figure 2A). By assessing Gag condensation, we estimated that ~75% of the VLPs, both gp120-VLPs and Env(-) VLPs, were mature. These percentages were lower for NL4-3ΔIN virions (~50%) and for immature VLPs (~16%) used as controls (Figure 2B). Furthermore, we observed that 26.5% of the gp120-VLPs, 40.2% of the NL4-3ΔIN virions, and 40.5% of the immature VLPs expressed gp120. As a control, the anti-gp120 2G12 Fab did not stain particles lacking the Env (Env(-) VLPs) (Figure 2A, C), confirming the specificity of the staining. Moreover, STED analysis revealed differences in Env distribution between gp120-VLPs and NL4-3ΔIN virions, as previously observed between mature and immature particles (13). Specifically, gp120 staining intensity was higher for NL4-3ΔIN particles than for gp120-VLPs (NL4-3ΔIN 1,786 a.u. vs. gp120-VLPs 1,223 a.u.) (Figure 2D), suggesting a lower expression of Env proteins in the latter or a lower incorporation of the Env proteins into the VLPs. Analysis of gp120 intensity per particle demonstrated that g120-VLPs had lower levels of gp120/particle than NL4-3ΔIN virions (Figure 2E). These data confirmed the mature state of the gp120-VLPs generated and indicated that they contained a reduced number of gp120/particle, similar to or even lower than that found in primary HIV-1 viruses (55).

Next, we employed SPT-TIRF to investigate how gp120-VLPs affect CXCR4 dynamics in JKCD4^{+}X4^{-} cells that were transiently transfected with CXCR4-AcGFP (Supplementary video 4-6). Analysis indicated that the gp120-VLPs significantly reduced overall receptor diffusivity (basal, D_{1-4} = 0.025 μm^2 s^{-1}; Env(-) VLPs, D_{1-4} = 0.017 μm^2 s^{-1}; gp120-VLPs D_{1-4} = 0.012 μm^2 s^{-1}) (Figure 3A). In all the cases, most of the trajectories corresponded to confined movement (Supplementary Figure 5B) Under these conditions, we found predominantly CXCR4 monomers and dimers at steady-state, and

their proportion decreased upon VLP treatment (basal ~99%; Env(-) VLPs ~91%; gp120-VLPs ~71%). Consequently, the percentage of nanoclusters containing ≥3 receptors/particle increased (~1%, basal; ~9%, VLPs; ~29%, gp120-VLPs) (Figure 3B). These findings were consistent with the MSI values (basal 761 a.u.; Env(-) VLPs 1,150 a.u.; gp120-VLPs 1,898 a.u.) (Figure 3C). Further investigations are needed to elucidate the precise mechanism involved in the effect induced by the Env(-) VLPs on the dynamics of the receptors.

Our results indicated that, similar to the effect triggered by soluble X4-gp120, VLPs containing HIV-1 Env also triggered CXCR4 nanoclustering. To understand the role of CXCR4 clustering in HIV-1 infection, we next analyzed the behavior of the WHIM mutant CXCR4, $CXCR4^{R334X}$, which does not oligomerize in the presence of CXCL12 (28). $CXCR4^{R334X}$ is a natural mutant of CXCR4 that binds CXCL12 (59–61), but is not internalized in response to the ligand; in fact, it is a gain-of-function receptor for this ligand (62). SPT-TIRF-M analysis of $JKCD4^{+}X4^{-}$ cells transiently transfected with $CXCR4^{R334X}$-AcGFP (Supplementary video 7-9) demonstrated that, unlike the effect described for CXCL12, the VLPs containing gp120 triggered $CXCR4^{R334X}$ oligomerization (basal MSI 669 a.u.; Env(-) VLPs MSI 909 a.u.; gp120-VLPs MSI 1,730 a.u.) (Figure 4A) and promoted a significant reduction in overall receptor diffusivity (basal, median D_{1-4} = 0.021 $\mu m^2 s^{-1}$; gp120-VLPs, median D_{1-4} = 0.014 $\mu m^2 s^{-1}$) (Figure 4B) without significant differences in the percentage of trajectories with distinct type of diffusion, again most of them exhibited confined movement (Supplementary Figure 5C). Furthermore, gp120-VLP binding reduced the percentage of $CXCR4^{R334X}$ monomers and dimers (steady-state ~99%; gp120-VLPs ~80%), while concurrently increasing the percentage of nanoclusters containing ≥3 receptors/particle (basal ~1%; gp120-VLPs ~20%) (Figure 4C).

All these data and other previously reported findings (28), indicate that CXCL12 triggers CXCR4 clustering at the cell membrane but does not induce $CXCR4^{R334X}$ oligomers. By contrast, gp120-VLPs binding stabilized CD4 complexes with both CXCR4 and $CXCR4^{R334X}$ and promoted oligomerization of both co-receptors. It is thus plausible that the conformation of CXCR4 and $CXCR4^{R334X}$ may differ between both experimental conditions.

CD4 expression alters the conformation adopted by CXCR4

Our results support a model where CXCL12 binds to either CXCR4 or $CXCR4^{R334X}$ (28). By contrast, X4-gp120, whether alone or within the viral context, associates these co-receptors when they are complexed with CD4. It is known that CD4/CXCR4 complexes might facilitate co-operative interactions with HIV-1 during viral adsorption and/or entry into human leukocytes (63).

To confirm the interaction between CD4 and CXCR4 (22) and to assess whether $CXCR4^{R334X}$ could also interact with CD4, we conducted FRET analyses. Our results demonstrated positive FRET signals for both complexes: CD4/CXCR4 ($FRET_{50}$=2.71) and CD4/$CXCR4^{R334X}$ ($FRET_{50}$=0.40) (Figure 5A, B). As a control, we observed minimal residual energy transfer in cells co-transfected with CD4-CFP and $5HT_{2B}$-YFP (Figure 5C). The presence of CD4/CXCR4 and CD4/$CXCR4^{R334X}$ heterodimers was also investigated *in silico* using alphaFold3 (64) (Supplementary Figure 7). We focused on the interaction between the transmembrane and intracellular fragments of CD4 and both CXCR4 and $CXCR4^{R334X}$. The predicted template modeling (pTM) scores for both complexes were close to 0.7, suggesting a reliable prediction of these interactions. The modeling also indicated a preferred association of CD4 with CXCR4 between transmembrane helices IV and V, although further analysis is needed to precisely determine the interaction site. These data align with previous reports demonstrating a

constitutive association between CD4 and CXCR4 that can influence HIV-1 infection (22, 65–68) and our results extend this observation to the naturally occurring CXCR4^{R334X} mutant. Furthermore, we observed increased FRET efficiency in both CD4-CXCR4 and CD4-CXCR4^{R334X} complexes upon gp120-VLPs binding (Figure 5D, E), confirming that the VLPs induce conformational changes in these heterodimers.

Productive HIV-1 infection of CD4^{+} cells markedly diminishes cell-surface expression of CD4 (69, 70). However, the impact on chemokine receptors is less clear. While some studies report a complete loss of CCR5 surface staining on cells chronically infected with R5 viruses (71) the effect on CXCR4 varies (71, 72). Using flow cytometry, we investigated how stimulation with X4-gp120 affects the cell-surface expression of CD4, CXCR4, and CXCR4^{R334X}. Consistent with previous findings (73), CXCL12 induced rapid internalization of CXCR4 without altering CXCR4^{R334X} levels at the cell surface. By contrast, X4-gp120 caused a gradual, slight decrease in the surface expression of both receptors. Furthermore, CXCL12 did not affect CD4 surface levels, whereas X4-gp120 induced a gradual decline in CD4 expression (Figure 6A, B).

Taken together, our FRET and internalization experiments suggest that the effects of X4-gp120 on CXCR4 and CXCR4^{R334X} differ from those triggered by CXCL12 and are dependent on their interaction with CD4.

Next, we investigated whether CD4/CXCR4^{R334X} complexes could also support primary HIV-1 infection. Flow cytometry analysis showed no significant difference in the ability of Jurkat cells expressing either CXCR4 or CXCR4^{R334X} to bind X4-gp120 (Figure 7A). In agreement, *in vitro* fusion assays using cells expressing CD4/CXCR4 or CD4/CXCR4^{R334X}, and target cells expressing HIV pHXB2 Env, demonstrated a significant increase in fusion events and syncytium formation in both Jurkat cell types (Figure 7B, C). We then tested whether PBMCs isolated from a WHIM patient and

healthy donors were equally susceptible to infection by a primary X4 HIV-1_{NL4-3} viral strain. We first analyzed the expression of CD4, and CXCR4 or $CXCR4^{R334X}$ on these PBMC samples by flow cytometry (Supplementary Figure 8A-C). Subsequently, cells were stimulated with PHA and IL-2, and 48 hours later, inoculated with a primary X4 HIV-1_{NL4-3} virus at a MOI of 0.001 for 120 minutes. ELISA measurements of p24 levels in the culture medium at various time points revealed similar viral infection rates in both Healthy and WHIM PBMCs (Figure 7D).

Collectively, these data indicate that T cells from a WHIM patient exhibit similar infection and viral replication rates with those isolated from healthy donors. Furthermore, these data suggest that HIV-1 might modulate the conformation adopted by CXCR4 at the cell membrane, which is associated with HIV-1 infection. The CXCR4 conformation stabilized by HIV-1 binding likely differs from that induced by CXCL12 binding and therefore supports a direct effect of the interactions with CD4 in establishing a permissive conformation of CXCR4 for HIV-1 infection.

Discussion

The process of HIV-1 infection begins with the binding of the trimeric HIV-1 Env glycoprotein to the CD4 receptor on the target cell surface (74–76). Research indicates that when the viral and cellular membranes are spatially distant, the HIV-1 Env trimers initially engage only a single CD4 molecule, and as the Env moves closer to the membrane and adopts an open conformation it gains the ability to bind a second and a third CD4 molecule (24). CD4 binding thus induces critical conformational changes within the gp120 subunit of Env that enable subsequent engagement of the co-receptors CCR5 or CXCR4. Receptor and co-receptor engagement trigger further conformational changes in the Env gp41 subunits, ultimately mediating the necessary fusion of the viral and host cell membranes.

Competitive receptor inhibitors, such as soluble synthetic CD4 (sCD4), synthetic CD4 peptides, and anti-CD4 binding site antibodies have been shown to effectively block infection both *in vitro* (77, 78) and *in vivo* (79, 80). Notably, virus-like nanoparticles displaying clustered membrane-associated CD4 demonstrated significantly greater efficacy at blocking infection compared with sCD4, CD4-Ig, or the broadly neutralizing monoclonal antibody 3BNC117 (81). These findings collectively suggest that the virus may induce CD4 clustering to promote cell infection. Consistent with this idea, single-molecule super-resolution imaging has revealed that CD4 molecules on the cell membrane exist predominantly as individual molecules or small clusters (up to 4 molecules), and that the size and number of these clusters increase upon virus binding or gp120 activation (19). These data therefore support a model where viral binding triggers a nanoscale reorganization of CD4 on the plasma membrane, a process necessary for cell infection. This observation aligns with substantial evidence indicating that various cell-surface receptors are organized into clusters (23, 82). For instance, T-cell receptors on T cells coalesce into nanoclusters within and around immune synapses prior to signal transduction (83, 84). Receptor clustering has been also demonstrated for numerous other transmembrane receptors, such as neurotransmitter receptors (85) and immune receptors (86, 87). Furthermore, studies analyzing receptor dynamics during cell movement using SPT have shown that chemokine-mediated receptor clustering is essential for cells to accurately sense chemoattractant gradients (27, 28).

Here, using SPT-TIRF-M analysis on Jurkat cells, we found that both recombinant X4-gp120 and VLPs displaying X4 HIV-1 Env (with fewer gp120 molecules) actively promote CXCR4 clustering and modify its membrane dynamics in a CD4-dependent manner. Our data show that, similar to the effect of CXCL12, gp120 binding to CXCR4 leads to a significant decrease in the number of monomers and dimers, while increasing

the proportion of larger, generally immobile nanoclusters. Previous studies utilizing immunoelectron microscopy have suggested that CCR5, CXCR4, and CD4 are mainly localized on microvilli and tend to form distinct, uniform microclusters in all cell types examined (63). This clustering is thought to enhance co-operative interactions with HIV-1 during virus adsorption and subsequent entry into human leukocytes (63). Single-molecule force spectroscopy has also revealed that the force and duration required to break apart the gp120/CCR5/CD4 complex are greater than those required for the gp120/CD4 bond (88). The formation of CCR5/CD4/CXCR4 oligomers is implicated in reducing the infectivity of X4 HIV-1 in cells that also express CCR5 (22).

The data suggest that exposure to HIV-1 triggers several rearrangements of cell receptors, highlighting the significance of these changes in facilitating viral entry into target cells. Receptor clustering, a process known to enhance cell sensitivity (89), also promotes efficient cell signal transmission (90), and increases the robustness of signaling systems (91). Indeed, it is well established that HIV-1 promotes CD4- and CXCR4-mediated signaling events that facilitate viral entry and infection of host cells (39, 92–95). We observed that gp120 triggered the phosphorylation of Lck, Akt, and ERK1/2, and promoted cell polarization, although this latter effect was less pronounced than that induced by CXCL12. Furthermore, in lipid bilayer assays using ICAM-1 as a substrate, gp120 mediated Jurkat cell adhesion but did not significantly promote cell migration compared with CXCL12. While soluble gp120 has been used to investigate certain HIV-1 effects on cells (39, 43, 96), employing saturating concentrations of the glycoprotein might lead to non-specific effects on the dynamics of receptors and co-receptors at the cell membrane. Moreover, the conformation of recombinant gp120 may not accurately reflect its physiological structure on intact HIV-1 particles. Within virions, the Env glycoprotein forms heterotrimeric gp120 non-covalently associated with three gp41

molecules. To address these limitations, we generated VLPs displaying the X4 HIV-1 Env. Super-resolution microscopy confirmed the maturity of the gp120-VLPs, expressing a very low number of gp120 trimers on their surface, even fewer than the 7 to 14 Env trimers per virus particle previously reported on primary isolated virions (54, 97, 98) Similar to soluble recombinant gp120, these VLPs also induced CXCR4 clustering and altered receptor dynamics. These findings thus confirm that the effects observed with X4-gp120 are not artifacts resulting from the conformation of the soluble gp120 or to the use of saturating concentrations. Receptor clustering was initiated through binding of gp120-VLPs to CD4 and CXCR4, as neither X4-gp120 nor the VLPs associated with CXCR4 in the absence of CD4. We confirmed this using a mutant CXCR4, $CXCR4^{R334X}$, which does not oligomerize in the presence of CXCL12 (28). $CXCR4^{R334X}$ is found in cells of patients with WHIM syndrome, a rare combined immunodeficiency characterized by the presence of warts, hypogammaglobulinemia, recurrent bacterial infections and myelokathexis symptoms (29). In these patients, the inability of CXCL12 to induce receptor oligomerization leads to defects in actin dynamics, preventing proper sensing of chemoattractant gradients (28, 99). We investigated how VLPs containing the X4 HIV-1 Env affected the dynamics of $CXCR4^{R334X}$ in cells expressing CD4. Surprisingly, the X4 HIV-1 Env caused a significant reduction in $CXCR4^{R334X}$ monomers and dimers, while increasing the proportion of larger nanoclusters, which were generally immobile. These findings suggest that CXCL12 and gp120 VLPs have different effects on chemokine receptor dynamics, leading us to hypothesize that the structure of CXCR4, whether or not it is associated with CD4, could explain these observations. AlphaFold predictions and FRET analysis confirmed the formation of CD4/CXCR4 complexes (22) and supported the existence of CD4/$CXCR4^{R334X}$ heterodimers. In both cases, gp120-VLPs binding altered the conformations. These findings correlate with the syncytia formation observed

in *in vitro* fusion experiments between cells expressing the X4 HIV-1 Env and target cells expressing either CD4/CXCR4 or CD4/CXCR4^{R334X}, and with the infection of PBMCs from both WHIM patients and healthy donors when incubated with primary X4-HIV-1. These findings also indicate that WHIM mutations do not protect against HIV-1 infection, consistent with a previous *in vitro* study showing that CD4^{+}U87 cells expressing CXCR4^{R334X} or CXCR4 are equally susceptible to a luciferase-expressing pseudotyped virus infection (60). To better reflect natural infection kinetics, we employed fully replication-competent viruses rather than pseudotyped systems. Furthermore, we monitored viral dynamics over a seven-day period, providing a longitudinal perspective that extends beyond the limitations of a standard 24-hour snapshot. Beyond inducing CXCR4 aggregation, we observed that X4-gp120 promoted the internalization of CD4 and CXCR4 and, surprisingly, also triggered the internalization of CXCR4^{R334X}. This mutant receptor cannot internalize in response to CXCL12 because it lacks the last 19 C-terminal amino acids, which are necessary for GRK-mediated Ser/Thr phosphorylation and β-arrestin recruitment (29, 100). Some studies suggest that HIV-1 glycoproteins can reduce CD4 and CXCR4 levels during HIV-1 entry (72, 101, 102), proposing receptor-mediated endocytosis as an alternative HIV-1 entry mechanism (103–108). Other reports even indicate a ligand-mediated co-endocytosis of CD4 and the chemokine receptors during HIV-1 entry (109–111). HIV-1-mediated endocytosis might also explain the reduction of CD4 and CXCR4^{R334X} at the cell membrane and the similar infection rates in PBMCs from WHIM patients and healthy donors. Although direct evidence for the internalization of CD4 and CXCR4 as complexes is lacking, their co-localization in lipid rafts during HIV-1 infection (32, 112, 113) and their ability to form heterocomplexes (22) strongly suggest they could be endocytosed together. Therefore, we hypothesize that

gp120 binding to CD4 stabilizes CD4/CXCR4 complexes, and that the conformation of CXCR4 within these complexes might differ from that of CXCR4 homodimers.

We also detected a residual but significant effect of Env(-) VLPs on the dynamics of both CXCR4 and of CXCR4^{R334X}. This is likely not receptor-mediated, as these control VLPs lacked the X4 HIV-1 Env. While further experiments are needed, a potential interaction between the lipids and or cell adhesion molecules derived from the cells where the virions were produced, and those in the cell membrane could explain this observation. It is well established that the lipid composition of the cell membrane influences ligand-mediated chemokine receptor oligomerization and dynamics (114, 115). Additionally, glycosaminoglycans, such as heparin and heparan sulphate, might play a role in the attachment of virions to various cell types (116–118). Although their effects on R5 strains are debated (119–121), the concentrations of these glycosaminoglycans vary considerably between cells (122). Besides, some viruses bind lectins at the cell membrane, for instance some microdomains of C-type lectin DC-SIGN have been described as portals for HIV-1 entry (123, 124).

Our data indicate that HIV-1 not only affects CD4 dynamics, which is well known, but also alters the spatial distribution and dynamics of CXCR4 in a manner distinct from the effects of its natural ligand, CXCL12. While HIV-1 binding involves CD4/CXCR4 complexes, CXCL12 binds exclusively to CXCR4, potentially leading to different effects on CXCR4 conformations. These findings might also explain why HIV-1 induced the endocytosis of both CD4/CXCR4 and CD4/CXCR4^{R334X} complexes, whereas CXCL12 did not mediate the internalization of either CD4 or the CD4/CXCR4^{R334X} complex. This suggests that the interaction of both co-receptors with CD4 may result in different conformations of CXCR4 and CXCR4^{R334X} compared with their respective homodimers. The interaction motif between CD4 and CXCR4 should be considered a crucial target for

disrupting complex dynamics at the cell membrane, potentially opening new avenues for anti-HIV-1 therapies.

Acknowledgements

This work was supported by grants from the Spanish Ministry of Science and Innovation (PID2020-114980RB-I00 and PID2023-146301OB-I00) to MM and (PID2022-140651NB-I00) to CS, and (PID2022-139271OB-I00 and CB21/13/00063) to JM-P. EG-C and BS were supported by the program Apoyos Centros de Excelencia S.O. of the Spanish Ministry of Science and Innovation (SEV-2017-0712). AQ-F and SRG ere included in the doctoral program of the Department of Molecular Biosciences and of Biology, respectively, Universidad Autónoma de Madrid, and are supported by the Fondo de Personal Investigador (FPI) program of the Spanish Ministry for Science and Innovation (PRE2018-083201 and PRE2019-087966, respectively). EAB is included in the doctoral program of Biomedicine, University of Barcelona, and is supported by the FPI program of the Spanish Ministry for Science and Innovation (PRE2022-000847). RA-B is supported by the Garantía Juvenil program of the Regional Government of Madrid, Spain (CAM20_CNB_AI_07). LIGG receives funding from Institute of Health, Carlos III co-funded by Fondos FEDER Project FIS PI21/01642. We also acknowledge the technical help of the Advance Light Microscopy Unit at the CNB/CSIC.

JMP has received research funding, consultancy fees, and lecture sponsorships from and has served on advisory boards for various companies (AbiVax, AstraZeneca, MSD, Gilead Sciences, ViiV Healthcare, Johnson & Johnson) outside the scope of this article. The rest of the authors declare no competing interests.

Bibliography

1. M. Kowalski, *et al.*, Functional regions of the envelope glycoprotein of human immunodeficiency virus type 1. *Science* 237, 1351–1355 (1987).
2. M. Lu, S. C. Blacklow, P. S. Kim, A trimeric structural domain of the HIV-1 transmembrane glycoprotein. *Nature Structural Biology 1995 2:12* 2, 1075–1082 (1995).
3. H. Choe, *et al.*, The beta-chemokine receptors CCR3 and CCR5 facilitate infection by primary HIV-1 isolates. *Cell* 85, 1135–1148 (1996).
4. Y. Feng, C. C. Broder, P. E. Kennedy, E. A. Berger, HIV-1 entry cofactor: functional cDNA cloning of a seven-transmembrane, G protein-coupled receptor. *Science* 272, 872–877 (1996).
5. S. M. Wolinsky, *et al.*, Adaptive evolution of human immunodeficiency virus-type 1 during the natural course of infection. *Science* 272, 537–542 (1996).
6. Z. H. Lu, *et al.*, Evolution of HIV-1 coreceptor usage through interactions with distinct CCR5 and CXCR4 domains. *Proc Natl Acad Sci U S A* 94, 6426–6431 (1997).
7. R. I. Connor, H. Mohri, Y. Cao, D. D. Ho, Increased viral burden and cytopathicity correlate temporally with CD4+ T-lymphocyte decline and clinical progression in human immunodeficiency virus type 1-infected individuals. *J Virol* 67, 1772–1777 (1993).
8. C. C. Carter, *et al.*, HIV-1 Utilizes the CXCR4 Chemokine Receptor to Infect Multipotent Hematopoietic Stem and Progenitor Cells. *Cell Host Microbe* 9, 223–234 (2011).
9. N. R. Landau, M. Warton, D. R. Littman, The envelope glycoprotein of the human immunodeficiency virus binds to the immunoglobulin-like domain of CD4. *Nature* 334, 159–162 (1988).
10. J. Arthos, *et al.*, Identification of the residues in human CD4 critical for the binding of HIV. *Cell* 57, 469–481 (1989).
11. W. Zhang, *et al.*, Conformational changes of gp120 in epitopes near the CCR5 binding site are induced by CD4 and a CD4 miniprotein mimetic. *Biochemistry* 38, 9405–9416 (1999).
12. R. W. Doms, J. P. Moore, HIV-1 membrane fusion: targets of opportunity. *J Cell Biol* 151 (2000).
13. J. Chojnacki, *et al.*, Maturation-dependent HIV-1 surface protein redistribution revealed by fluorescence nanoscopy. *Science* 338, 524–528 (2012).
14. V. Buzon, *et al.*, Crystal structure of HIV-1 gp41 including both fusion peptide and membrane proximal external regions. *PLoS Pathog* 6, 1–7 (2010).
15. M. Pancera, *et al.*, Structure of HIV-1 gp120 with gp41-interactive region reveals layered envelope architecture and basis of conformational mobility. *Proc Natl Acad Sci U S A* 107, 1166–1171 (2010).
16. H. Garg, M. Viard, A. Jacobs, R. Blumenthal, Targeting HIV-1 gp41-induced fusion and pathogenesis for anti-viral therapy. *Curr Top Med Chem* 11, 2947–2958 (2011).
17. M. Barrero-Villar, *et al.*, Moesin is required for HIV-1-induced CD4-CXCR4 interaction, F-actin redistribution, membrane fusion and viral infection in lymphocytes. *J Cell Sci* 122, 103–113 (2009).
18. S. Jiménez-Baranda, *et al.*, Filamin-A regulates actin-dependent clustering of HIV receptors. *Nat Cell Biol* 9, 838–846 (2007).
19. Y. Yuan, *et al.*, Single-Molecule Super-Resolution Imaging of T-Cell Plasma Membrane CD4 Redistribution upon HIV-1 Binding. *Viruses* 13 (2021).

20. C. K. Lapham, *et al.*, Evidence for cell-surface association between fusin and the CD4-gp120 complex in human cell lines. *Science* 274, 602–605 (1996).
21. S. Ugolini,', *et al.*, HIV-1 gp120 Induces an Association Between CD4 and the Chemokine Receptor CXCR4'. *The Journal of Immunology* 159, 3000–3008 (1997).
22. L. Martínez-Muñoz, *et al.*, CCR5/CD4/CXCR4 oligomerization prevents HIV-1 gp120IIIB binding to the cell surface. *Proc Natl Acad Sci U S A* 111 (2014).
23. N. C. Hartman, J. T. Groves, Signaling clusters in the cell membrane. *Curr Opin Cell Biol* 23, 370–376 (2011).
24. W. Li, *et al.*, HIV-1 Env trimers asymmetrically engage CD4 receptors in membranes. *Nature* 623, 1026–1033 (2023).
25. M. F. Krummel, M. D. Sjaastad, C. W. Wulfing, M. M. Davis, Differential clustering of CD4 and CD3zeta during T cell recognition. *Science* 289, 1349–1352 (2000).
26. H. Kao, J. Lin, D. R. Littman, A. S. Shaw, P. M. Allen, Regulated movement of CD4 in and out of the immunological synapse. *J Immunol* 181, 8248–8257 (2008).
27. L. Martínez-Muñoz, *et al.*, Separating Actin-Dependent Chemokine Receptor Nanoclustering from Dimerization Indicates a Role for Clustering in CXCR4 Signaling and Function. *Mol Cell* 70, 106-119.e10 (2018).
28. E. M. García-Cuesta, *et al.*, Altered CXCR4 dynamics at the cell membrane impairs directed cell migration in WHIM syndrome patients. *Proc Natl Acad Sci U S A* 119 (2022).
29. Q. Liu, *et al.*, WHIM syndrome caused by a single amino acid substitution in the carboxy-tail of chemokine receptor CXCR4. *Blood* 120, 181–189 (2012).
30. E. M. García-Cuesta, *et al.*, Altered CXCR4 dynamics at the cell membrane impairs directed cell migration in WHIM syndrome patients. *Proc Natl Acad Sci U S A* 119 (2022).
31. S. R. Gardeta, *et al.*, Sphingomyelin Depletion Inhibits CXCR4 Dynamics and CXCL12-Mediated Directed Cell Migration in Human T Cells. *Front Immunol* 13 (2022).
32. S. Mañes, *et al.*, Membrane raft microdomains mediate lateral assemblies required for HIV-1 infection. *EMBO Rep* 1, 190–196 (2000).
33. L. Martínez-Muñoz, *et al.*, Separating Actin-Dependent Chemokine Receptor Nanoclustering from Dimerization Indicates a Role for Clustering in CXCR4 Signaling and Function. *Mol Cell* 70, 106-119.e10 (2018).
34. G. Del Real, *et al.*, Blocking of HIV-1 infection by targeting CD4 to nonraft membrane domains. *J Exp Med* 196, 293–301 (2002).
35. Y. R. Carrasco, S. J. Fleire, T. Cameron, M. L. Dustin, F. D. Batista, LFA-1/ICAM-1 interaction lowers the threshold of B cell activation by facilitating B cell adhesion and synapse formation. *Immunity* 20, 589–599 (2004).
36. L. Martínez Muñoz, *et al.*, Dynamic regulation of CXCR1 and CXCR2 homo- and heterodimers. *J Immunol* 183, 7337–7346 (2009).
37. K. Jaqaman, *et al.*, Robust single-particle tracking in live-cell time-lapse sequences. *Nat Methods* 5, 695–702 (2008).
38. S. Dorsch, K. N. Klotz, S. Engelhardt, M. J. Lohse, M. Bünemann, Analysis of receptor oligomerization by FRAP microscopy. *Nat Methods* 6, 225–230 (2009).
39. K. Balabanian, *et al.*, CXCR4-Tropic HIV-1 Envelope Glycoprotein Functions as a Viral Chemokine in Unstimulated Primary CD4 + T Lymphocyteskk. *The Journal of Immunology* 173, 7150–7160 (2004).

40. J. Arthos, *et al.*, CCR5 signal transduction in macrophages by human immunodeficiency virus and simian immunodeficiency virus envelopes. *J Virol* 74, 6418–6424 (2000).
41. G. Briand, B. Barbeau, M. Tremblay, Binding of HIV-1 to its receptor induces tyrosine phosphorylation of several CD4-associated proteins, including the phosphatidylinositol 3-kinase. *Virology* 228, 171–179 (1997).
42. A. P. Curnock, M. K. Logan, S. G. Ward, Chemokine signalling: pivoting around multiple phosphoinositide 3-kinases. *Immunology* 105, 125–136 (2002).
43. A. Yoder, *et al.*, HIV Envelope-CXCR4 Signaling Activates Cofilin to Overcome Cortical Actin Restriction in Resting CD4 T Cells. *Cell* 134, 782–792 (2008).
44. S. Iyengar, J. E. K. Hildreth, D. H. Schwartz, Actin-dependent receptor colocalization required for human immunodeficiency virus entry into host cells. *J Virol* 72, 5251–5255 (1998).
45. A. G. Bukrinskaya, HIV-1 assembly and maturation. *Arch Virol* 149, 1067–1082 (2004).
46. S. J. Plowman, C. Muncke, R. G. Parton, J. F. Hancock, H-ras, K-ras, and inner plasma membrane raft proteins operate in nanoclusters with differential dependence on the actin cytoskeleton. *Proc Natl Acad Sci U S A* 102, 15500–15505 (2005).
47. J. A. Torreno-Pina, *et al.*, The actin cytoskeleton modulates the activation of iNKT cells by segregating CD1d nanoclusters on antigen-presenting cells. *Proc Natl Acad Sci U S A* 113, E772–E781 (2016).
48. P. M. Pereira, *et al.*, Fix Your Membrane Receptor Imaging: Actin Cytoskeleton and CD4 Membrane Organization Disruption by Chemical Fixation. *Front Immunol* 10 (2019).
49. C. Manzo, M. F. Garcia-Parajo, A review of progress in single particle tracking: From methods to biophysical insights. *Reports on Progress in Physics* [Preprint] (2015). Available at: http://www.ncbi.nlm.nih.gov/pubmed/26511974 [Accessed 11 January 2022].
50. H. Ewers, *et al.*, Single-particle tracking of murine polyoma virus-like particles on live cells and artificial membranes. *Proc Natl Acad Sci U S A* 102, 15110–15115 (2005).
51. D. Calebiro, *et al.*, Single-molecule analysis of fluorescently labeled G-protein-coupled receptors reveals complexes with distinct dynamics and organization. *Proc Natl Acad Sci U S A* 110, 743–748 (2013).
52. J. Chojnacki, *et al.*, Envelope glycoprotein mobility on HIV-1 particles depends on the virus maturation state. *Nat Commun* 8 (2017).
53. T. K. Hart, A. M. Klinkner, J. Ventre, P. J. Bugelski, Morphometric analysis of envelope glycoprotein gp120 distribution on HIV-1 virions. *J Histochem Cytochem* 41, 265–271 (1993).
54. P. Zhu, *et al.*, Electron tomography analysis of envelope glycoprotein trimers on HIV and simian immunodeficiency virus virions. *Proc Natl Acad Sci U S A* 100, 15812–15817 (2003).
55. P. Zhu, *et al.*, Distribution and three-dimensional structure of AIDS virus envelope spikes. *Nature* 441, 847–852 (2006).
56. T. Murakami, S. Ablan, E. O. Freed, Y. Tanaka, Regulation of human immunodeficiency virus type 1 Env-mediated membrane fusion by viral protease activity. *J Virol* 78, 1026–1031 (2004).

57. D. J. Wyma, *et al.*, Coupling of human immunodeficiency virus type 1 fusion to virion maturation: a novel role of the gp41 cytoplasmic tail. *J Virol* 78, 3429–3435 (2004).
58. N. R. Rauh, A. Schmidt, J. Bormann, E. A. Nigg, T. U. Mayer, Calcium triggers exit from meiosis II by targeting the APC/C inhibitor XErp1 for degradation. *Nature* 437, 1048–1052 (2005).
59. K. Balabanian, *et al.*, WHIM syndromes with different genetic anomalies are accounted for by impaired CXCR4 desensitization to CXCL12. *Blood* 105, 2449–2457 (2005).
60. P. A. Hernandez, *et al.*, Mutations in the chemokine receptor gene CXCR4 are associated with WHIM syndrome, a combined immunodeficiency disease. *Nat Genet* 34, 70–74 (2003).
61. J. M. Busillo, J. L. Benovic, Regulation of CXCR4 signaling. *Biochim Biophys Acta* 1768, 952–963 (2007).
62. D. H. Mcdermott, *et al.*, AMD3100 is a potent antagonist at CXCR4(R334X) , a hyperfunctional mutant chemokine receptor and cause of WHIM syndrome. *J Cell Mol Med* 15, 2071–2081 (2011).
63. I. I. Singer, *et al.*, CCR5, CXCR4, and CD4 are clustered and closely apposed on microvilli of human macrophages and T cells. *J Virol* 75, 3779–3790 (2001).
64. J. Abramson, *et al.*, Accurate structure prediction of biomolecular interactions with AlphaFold 3. *Nature* 630, 493–500 (2024).
65. S. Basmaciogullari, B. Pacheco, S. Bour, J. Sodroski, Specific interaction of CXCR4 with CD4 and CD8alpha: functional analysis of the CD4/CXCR4 interaction in the context of HIV-1 envelope glycoprotein-mediated membrane fusion. *Virology* 353, 52–67 (2006).
66. M. Zaitseva, *et al.*, Increased CXCR4-dependent HIV-1 fusion in activated T cells: role of CD4/CXCR4 association. *J Leukoc Biol* 78, 1306–1317 (2005).
67. C. K. Lapham, M. B. Zaitseva, S. Lee, T. Romanstseva, H. Golding, Fusion of monocytes and macrophages with HIV-1 correlates with biochemical properties of CXCR4 and CCR5. *Nat Med* 5, 303–308 (1999).
68. S. Lee, *et al.*, Coreceptor competition for association with CD4 may change the susceptibility of human cells to infection with T-tropic and macrophagetropic isolates of human immunodeficiency virus type 1. *J Virol* 74, 5016–5023 (2000).
69. J. A. Hoxie, *et al.*, Alterations in T4 (CD4) protein and mRNA synthesis in cells infected with HIV. *Science* 234, 1123–1127 (1986).
70. Viral interference in HIV-1 infected cells - Potash - 1998 - Reviews in Medical Virology - Wiley Online Library. Available at: https://onlinelibrary.wiley.com/doi/pdf/10.1002/(SICI)1099-1654(1998100)8:4%3C203::AID-RMV224%3E3.0.CO;2-%23 [Accessed 28 March 2025].
71. A. L. Chenine, Q. Sattentau, M. Moulard, Selective HIV-1-induced downmodulation of CD4 and coreceptors. *Arch Virol* 145, 455–471 (2000).
72. B. Choi, *et al.*, Down-regulation of cell surface CXCR4 by HIV-1. *Virol J* 5 (2008).
73. K. Balabanian, B. Lagane, J. Pablos, L. L.- Blood, undefined 2005, WHIM syndromes with different genetic anomalies are accounted for by impaired CXCR4 desensitization to CXCL12. *ashpublications.orgK Balabanian, B Lagane, JL Pablos, L Laurent, T Planchenault, O Verola, C Lebbe, D KerobBlood, 2005•ashpublications.org*.

74. R. Wyatt, J. Sodroski, The HIV-1 envelope glycoproteins: fusogens, antigens, and immunogens. *Science* 280, 1884–1888 (1998).
75. R. Blumenthal, S. Durell, M. Viard, HIV entry and envelope glycoprotein-mediated fusion. *J Biol Chem* 287, 40841–40849 (2012).
76. B. Chen, Molecular Mechanism of HIV-1 Entry. *Trends Microbiol* 27, 878–891 (2019).
77. A. Traunecker, J. Schneider, H. Kiefer, K. Karjalainen, Highly efficient neutralization of HIV with recombinant CD4-immunoglobulin molecules. *Nature* 339, 68–70 (1989).
78. P. L. Nara, K. M. Hwang, D. M. Rausch, J. D. Lifson, L. E. Eiden, CD4 antigen-based antireceptor peptides inhibit infectivity of human immunodeficiency virus in vitro at multiple stages of the viral life cycle. *Proc Natl Acad Sci U S A* 86, 7139–7143 (1989).
79. R. T. Schooley, *et al.*, Recombinant soluble CD4 therapy in patients with the acquired immunodeficiency syndrome (AIDS) and AIDS-related complex. A phase I-II escalating dosage trial. *Ann Intern Med* 112, 247–253 (1990).
80. J. O. Kahn, *et al.*, The safety and pharmacokinetics of recombinant soluble CD4 (rCD4) in subjects with the acquired immunodeficiency syndrome (AIDS) and AIDS-related complex. A phase 1 study. *Ann Intern Med* 112, 254–261 (1990).
81. M. A. G. Hoffmann, *et al.*, Nanoparticles presenting clusters of CD4 expose a universal vulnerability of HIV-1 by mimicking target cells. *Proc Natl Acad Sci U S A* 117, 18719–18728 (2020).
82. W. W. A. Schamel, B. Alarcón, Organization of the resting TCR in nanoscale oligomers. *Immunol Rev* 251, 13–20 (2013).
83. Y. Razvag, *et al.*, T Cell Activation through Isolated Tight Contacts. *Cell Rep* 29, 3506-3521.e6 (2019).
84. B. F. Lillemeier, *et al.*, TCR and Lat are expressed on separate protein islands on T cell membranes and concatenate during activation. *Nat Immunol* 11, 90–96 (2010).
85. P. Verstreken, H. J. Bellen, Meaningless minis? Mechanisms of neurotransmitter-receptor clustering. *Trends Neurosci* 25, 383–385 (2002).
86. R. N. Germain, T-cell signaling: the importance of receptor clustering. *Curr Biol* 7 (1997).
87. C. W. Cairo, Signaling by committee: receptor clusters determine pathways of cellular activation. *ACS Chem Biol* 2, 652–655 (2007).
88. M. I. Chang, P. Panorchan, T. M. Dobrowsky, Y. Tseng, D. Wirtz, Single-molecule analysis of human immunodeficiency virus type 1 gp120-receptor interactions in living cells. *J Virol* 79, 14748–14755 (2005).
89. D. Bray, Protein molecules as computational elements in living cells. *Nature* 376, 307–312 (1995).
90. W. Cho, R. V. Stahelin, Membrane-protein interactions in cell signaling and membrane trafficking. *Annu Rev Biophys Biomol Struct* 34, 119–151 (2005).
91. T. Gurry, O. Kahramanoğullari, R. G. Endres, Biophysical mechanism for ras-nanocluster formation and signaling in plasma membrane. *PLoS One* 4 (2009).
92. W. Popik, J. E. Hesselgesser, P. M. Pitha, Binding of human immunodeficiency virus type 1 to CD4 and CXCR4 receptors differentially regulates expression of inflammatory genes and activates the MEK/ERK signaling pathway. *J Virol* 72, 6406–6413 (1998).
93. C. B. Davis, *et al.*, Signal transduction due to HIV-1 envelope interactions with chemokine receptors CXCR4 or CCR5. *J Exp Med* 186, 1793–1798 (1997).

94. S. Pasquereau, G. Herbein, CounterAKTing HIV: Toward a “Block and Clear” Strategy? *Front Cell Infect Microbiol* 12 (2022).
95. F. François, M. E. Klotman, Phosphatidylinositol 3-kinase regulates human immunodeficiency virus type 1 replication following viral entry in primary CD4+ T lymphocytes and macrophages. *J Virol* 77, 2539–2549 (2003).
96. J. Deng, *et al.*, HIV Envelope gp120 Alters T Cell Receptor Mobilization in the Immunological Synapse of Uninfected CD4 T Cells and Augments T Cell Activation. *J Virol* 90, 10513–10526 (2016).
97. E. Chertova, *et al.*, Envelope glycoprotein incorporation, not shedding of surface envelope glycoprotein (gp120/SU), Is the primary determinant of SU content of purified human immunodeficiency virus type 1 and simian immunodeficiency virus. *J Virol* 76, 5315–5325 (2002).
98. M. C. DeSantis, J. H. Kim, H. Song, P. J. Klasse, W. Cheng, Quantitative Correlation between Infectivity and Gp120 Density on HIV-1 Virions Revealed by Optical Trapping Virometry. *J Biol Chem* 291, 13088–13097 (2016).
99. E. M. García-Cuesta, *et al.*, Allosteric modulation of the CXCR4:CXCL12 axis by targeting receptor nanoclustering via the TMV-TMVI domain. *Elife* 13 (2024).
100. R. Kumar, *et al.*, Reduced G protein signaling despite impaired internalization and β-arrestin recruitment in patients carrying a CXCR4Leu317fsX3 mutation causing WHIM syndrome. *JCI Insight* 8 (2023).
101. R. Geleziunas, S. Bour, M. A. Wainberg, Cell surface down-modulation of CD4 after infection by HIV-1. *FASEB J* 8, 593–600 (1994).
102. P. Hubert, G. Bismuth, M. Körner, P. Debré, HIV-1 glycoprotein gp120 disrupts CD4-p56lck/CD3-T cell receptor interactions and inhibits CD3 signaling. *Eur J Immunol* 25, 1417–1425 (1995).
103. J. Daecke, O. T. Fackler, M. T. Dittmar, H.-G. Kräusslich, Involvement of clathrin-mediated endocytosis in human immunodeficiency virus type 1 entry. *J Virol* 79, 1581–1594 (2005).
104. A. Aggarwal, *et al.*, HIV infection is influenced by dynamin at 3 independent points in the viral life cycle. *Traffic* 18, 392–410 (2017).
105. M. de la Vega, *et al.*, Inhibition of HIV-1 endocytosis allows lipid mixing at the plasma membrane, but not complete fusion. *Retrovirology* 8, 99 (2011).
106. K. Miyauchi, Y. Kim, O. Latinovic, V. Morozov, G. B. Melikyan, HIV enters cells via endocytosis and dynamin-dependent fusion with endosomes. *Cell* 137, 433–444 (2009).
107. G. C. Carter, L. Bernstone, D. Baskaran, W. James, HIV-1 infects macrophages by exploiting an endocytic route dependent on dynamin, Rac1 and Pak1. *Virology* 409, 234–250 (2011).
108. B. Van Wilgenburg, M. D. Moore, W. S. James, S. A. Cowley, The productive entry pathway of HIV-1 in macrophages is dependent on endocytosis through lipid rafts containing CD4. *PLoS One* 9 (2014).
109. M. Toyoda, *et al.*, Differential Ability of Primary HIV-1 Nef Isolates To Downregulate HIV-1 Entry Receptors. *J Virol* 89, 9639–9652 (2015).
110. S. Venzke, N. Michel, I. Allespach, O. T. Fackler, O. T. Keppler, Expression of Nef downregulates CXCR4, the major coreceptor of human immunodeficiency virus, from the surfaces of target cells and thereby enhances resistance to superinfection. *J Virol* 80, 11141–11152 (2006).

111. L.-A. Gobeil, R. Lodge, M. J. Tremblay, Macropinocytosis-like HIV-1 internalization in macrophages is CCR5 dependent and leads to efficient but delayed degradation in endosomal compartments. *J Virol* 87, 735–745 (2013).
112. W. Popik, T. M. Alce, W.-C. Au, Human immunodeficiency virus type 1 uses lipid raft-colocalized CD4 and chemokine receptors for productive entry into CD4(+) T cells. *J Virol* 76, 4709–4722 (2002).
113. N. F. Neel, E. Schutyser, J. Sai, G. H. Fan, A. Richmond, Chemokine receptor internalization and intracellular trafficking. *Cytokine Growth Factor Rev* 16, 637–658 (2005).
114. S. R. Gardeta, *et al.*, Sphingomyelin Depletion Inhibits CXCR4 Dynamics and CXCL12-Mediated Directed Cell Migration in Human T Cells. *Front Immunol* 13 (2022).
115. M. A. Hauser, *et al.*, Inflammation-Induced CCR7 Oligomers Form Scaffolds to Integrate Distinct Signaling Pathways for Efficient Cell Migration. *Immunity* 44, 59–72 (2016).
116. H. A. Harrop, C. C. Rider, Heparin and its derivatives bind to HIV-1 recombinant envelope glycoproteins, rather than to recombinant HIV-1 receptor, CD4. *Glycobiology* 8, 131–137 (1998).
117. I. Mondor, S. Ugolini, Q. J. Sattentau, Human immunodeficiency virus type 1 attachment to HeLa CD4 cells is CD4 independent and gp120 dependent and requires cell surface heparans. *J Virol* 72, 3623–3634 (1998).
118. A. C. S. Saphire, M. D. Bobardt, Z. Zhang, G. David, P. A. Gallay, Syndecans serve as attachment receptors for human immunodeficiency virus type 1 on macrophages. *J Virol* 75, 9187–9200 (2001).
119. M. Moulard, *et al.*, Selective interactions of polyanions with basic surfaces on human immunodeficiency virus type 1 gp120. *J Virol* 74, 1948–1960 (2000).
120. S. Ugolini, I. Mondor, Q. J. Sattentau, HIV-1 attachment: another look. *Trends Microbiol* 7, 144–149 (1999).
121. T. M. Dobrowsky, Y. Zhou, S. X. Sun, R. F. Siliciano, D. Wirtz, Monitoring early fusion dynamics of human immunodeficiency virus type 1 at single-molecule resolution. *J Virol* 82, 7022–7033 (2008).
122. D. L. Rabenstein, Heparin and heparan sulfate: structure and function. *Nat Prod Rep* 19, 312–331 (2002).
123. A. Cambi, *et al.*, Microdomains of the C-type lectin DC-SIGN are portals for virus entry into dendritic cells. *J Cell Biol* 164, 145–155 (2004).
124. L. Wu, V. N. KewalRamani, Dendritic-cell interactions with HIV: infection and viral dissemination. *Nat Rev Immunol* 6, 859–868 (2006).

Figure Legends

Figure 1. X4-gp120 modulates CXCR4 dynamics and nanoclustering. Single-particle tracking analysis of JKCD4^{+}X4^{-} cells transiently transfected with CXCR4-AcGFP on fibronectin (FN)-, FN + CXCL12-, or FN + X4-gp120-coated coverslips (828 particles in 96 cells on FN; 2,997 in 95 cells on FN + CXCL12 and 1,547 in 91 cells on FN + X4-gp120) n = 3. **A)** Percentage of mobile and immobile CXCR4-AcGFP particles at the

membrane of cells treated as indicated. **B)** Diffusion coefficients (D_{1-4}) of mobile particles at the membrane of cells treated as indicated with the median value of each experiment (black circles) and the median of all trajectories (dotted black lines). (****p ≤ 0.0001). **C)** Frequency of CXCR4-AcGFP particles containing monomers and dimers (≤2) or nanoclusters (≥3), mean ± SD calculated from mean spot intensity (MSI) values of each particle as compared with the value of monomeric CD86-AcGFP (980 ± 86 a.u., **p ≤ 0.01, ***p ≤ 0.001). **D)** Intensity distribution of individual CXCR4-AcGFP trajectories on unstimulated and CXCL12 or X4-gp120-stimulated cells. Graph shows the distribution of all trajectories, with the mean value of each experiment (black circles) and the median of all trajectories (dotted black lines) (n = 3; ****p ≤ 0.0001). Statistical significance was determined by two-way ANOVA in panels A and C and by non-parametric Kruskal-Wallis tests followed by Dunn's test for panels B and D.

Figure 2. gp120-VLPs are mature particles that express a low number of Env trimers. A) Representative images of clarified VLPs visualized by STED microscopy. Upper panels show images of the indicated VLPs stained for Gag p24 (blue) and gp120 (red). Lower panels show 10× magnification of equivalent images. White arrows indicate mature VLPs (p24 condensation). (**B)** Percentage of mature VLPs, analyzed from the images in A) using TrackAnalyzer in ImageJ, based on p24 intensity and aggregation level (mean ± SD; n = 2; ****p ≤ 0.0001; the significance indicated on immature VLPs bar shows the difference with all other conditions). **C)** Percentage of VLPs expressing gp120 on their surface, as analyzed in ImageJ (mean ± SD; n = 2; ***p ≤ 0.001). **D)** Distribution of gp120 mean fluorescence intensity. Each spot corresponds to the mean fluorescence intensity for each analyzed VLP in a.u. The black line represents the mean of all values (****p ≤ 0.0001). **E)** Frequency of gp120 intensity/particle. Statistical significance was determined by one-way-ANOVA followed by Tukey's multiple comparisons test in panels B and C and by Mann-Whitney analysis for panel D.

Figure 3. gp120 VLPs modulate CXCR4 dynamics and nanoclustering. Single-particle tracking analysis of $JKCD4^{+}X4^{-}$ cells transiently transfected with CXCR4-AcGFP, on fibronectin (FN)-, FN + VLPs-, or FN + gp120 VLPs-coated coverslips (1,087 particles in 159 cells on FN; 1,400 in 153 cells on FN +VLPs and 1,061 in 160 cells on

FN + gp120 VLPs) n = 6. **A)** Diffusion coefficients (D_{1-4}) of mobile particles at the membrane of cells treated as indicated. Figure shows the mean value of each experiment (black circles) and the median of all trajectories (dotted black lines) (n = 6; ****p ≤ 0.0001). **B)** Frequency of CXCR4-AcGFP particles containing monomers and dimers (≤2) or nanoclusters (≥3) in cells treated as indicated. Mean ± SD calculated from mean spot intensity (MSI) values of each particle as compared with the value of monomeric CD86-AcGFP (980 ± 86 a.u., **p ≤ 0.05, **p ≤ 0.01, ****p ≤ 0.0001). **C)** Intensity distribution (arbitrary units, a.u.) from individual CXCR4-AcGFP trajectories on cells treated as indicated. Graph shows the distribution of all trajectories, with the mean value of each experiment (black circles) and the median of all trajectories (dotted black lines) (n = 6; ****p ≤ 0.0001). Statistical significance was determined by non-parametric Kruskal-Wallis tests followed by Dunn's test for panels A and C, and by two-way ANOVA in panel B.

Figure 4. gp120 VLPs modulate CXCR4^{R334X} dynamics and nanoclustering. Single-particle tracking analysis of JKCD4^{+}X4^{-} cells transiently transfected with CXCR4^{R334X}-AcGFP, on fibronectin (FN)-, FN + VLPs-, or FN + gp120 VLPs-coated coverslips (341 particles in 63 cells on FN; 610 in 54 cells on FN + VLPs and 707 in 63 cells on FN + gp120 VLPs) n = 2. **A)** Intensity distribution (arbitrary units, a.u.) from individual CXCR4^{R334X}-AcGFP trajectories on cells treated as indicated. Graph shows the distribution of all trajectories, with the mean value of each experiment (black circles) and the median of all trajectories ± SD (dotted black lines) (n = 2; ****p ≤ 0.0001). **B)** Diffusion coefficients (D_{1-4}) of mobile single particle trajectories at the membrane of cells treated as indicated. Figure shows the mean value of each experiment (black circles) and the median of all trajectories (dotted black lines) (n = 2; n.s. not significant, *p ≤ 0.05, ****p ≤ 0.0001). **C)** Frequency of CXCR4^{R334X}-AcGFP particles containing monomers plus dimers (≤2) or nanoclusters (≥3), ± SD calculated from mean spot intensity values of each particle as compared with the value of monomeric CD86-AcGFP (*p ≤ 0.05, ***p ≤ 0.001). Statistical significance was determined by non-parametric Kruskal-Wallis tests followed by Dunn's test for panels A and C, and by two-way ANOVA in panel B.

Figure 5. CD4 forms heterodimers with CXCR4 and CXCR4^{R334X}. FRET saturation curves generated using HEK-293T cells transiently transfected with a constant amount of CD4-CFP DNA (2 μg) and increasing amounts of **A)** CXCR4-YFP (0.5–8.0 μg), **B)** CXCR4^{R334X}-YFP (0.5–8.0 μg) or **C)** $5HT_{2B}$ DNA (0.5–12 μg). K_D and $FRET_{max}$ values were calculated using a nonlinear regression equation for a single binding-site model (n = 2). **D)** FRET efficiency in HEK-293 cells transiently transfected with CXCR4-YFP/ CD4-CFP (ratio 15:9), in the absence or presence of gp120 VLPs or Env(-) VLPs. Data shows FRET efficiency (arbitrary units, a.u.) (mean ± SD; n = 3; n.s. not significant, *p ≤ 0.05, ***p ≤ 0.001). **E)** FRET efficiency in HEK-293 cells transiently transfected with CXCR4^{R334X}-YFP/CD4-CFP (ratio 15:9), in the absence or presence of gp120-VLPs or Env(-) VLPs. Data shows FRET efficiency (a.u.) (mean ± SD; n = 3; n.s. not significant, *p ≤ 0.05, ***p ≤ 0.001, ****p ≤ 0.0001). Statistical significance was determined by unpaired t-test in panels D and E.

Figure 6. X4-gp120 promote similar internalization patterns of CXCR4 and CXCR4^{R334X} receptors. A) Surface receptor expression of CXCR4 (white dots) or CXCR4^{R334X} (black dots), after stimulation with CXCL12 (blue lines) or X4-gp120 (red lines). Results show mean ± SD of the percentage of receptor expression at the cell surface (n = 3). **B)** Surface receptor expression of CD4 in JK CD4^{+} CXCR4^{+} (white dots) or JK CD4^{+} CXCR4^{R334X} (black dots), after stimulation with CXCL12 (blue lines) or X4-gp120 (red lines). Results show mean ± SD of the percentage of receptor expression at the cell surface (n = 3). Statistical significance was determined by one-way-ANOVA of AUC (*p ≤ 0.05, **p ≤ 0.01).

Figure 7. CD4/CXCR4 and CD4/CXCR4^{R334X} complexes support similar HIV-1 infection. The presence of CXCR4^{R334X} on JKCD4^{+} cells does not alter gp120 binding and increases fusion events with target cells expressing HIV pHXB2 envelope. **A)** Binding of X4-gp120 to target cells expressing CD4 and CXCR4 or CD4 and CXCR4^{R334X} analyzed by flow cytometry. Cells were incubated with 0.3 μg/mL of X4-gp120 at 37ºC for 30 minutes. Data show MFI (arbitrary units, a.u.) mean ± SD; (n = 2). Statistical significance was determined using Student's t-test (n.s.= not significant). **B)** Cell-cell fusion between JKHXBc2-expressing HIV-1 envelope and different target cells (JKCD4^{+}CXCR4^{+}, JKCD4^{+}CXCR4^{-} and JKCD4^{+}CXCR4^{R334X}). Prior to co-culture, each

cell type was loaded with the corresponding cell-tracker. Data show the percentage of fusion events ± SD (n = 6). We used as reference the fusions events detected in JKCD4^{+}CXCR4^{+} cells (100%). Statistical significance was determined by one-way-ANOVA (*$p < 0.05$, ****$p \leq 0.0001$). **C**) Representative biparametric histograms from cells in B showing CMAC *versus* orange fluorophores. **D**) Human PBMCs isolated from a WHIM patient (WHIM) and three healthy donors (HD1-3) in two independent experiments were infected with X4-pseudotyped HIV-1_{NL4-3} (MOI: 0.001). At 2 hours post infection (p.i.), supernatant samples were obtained at different time points (days post-infection) and p24 levels (pg/mL) in each sample were determined using a commercial ELISA. Results show mean ± SD (n = 2).

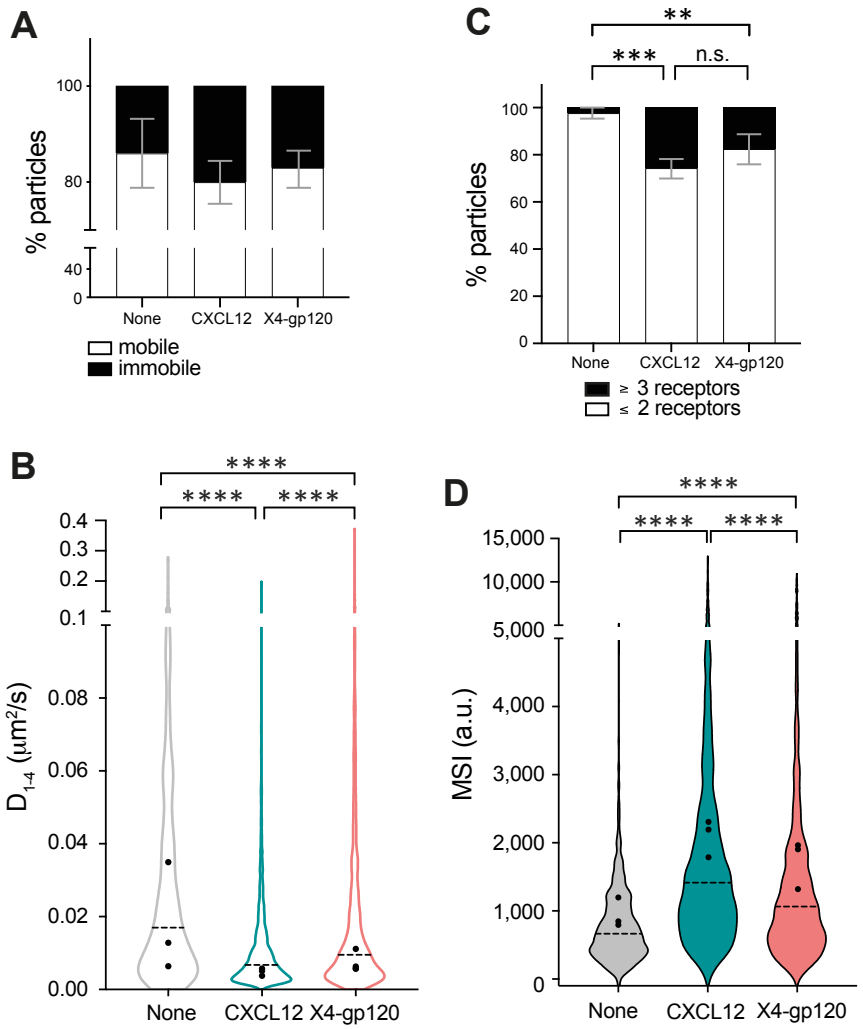
A
% particles
100
80
40
0
None
CXCL12
X4-gp120
mobile
immobile
C
**
***
n.s.
% particles
100
80
60
40
20
0
None
CXCL12
X4-gp120
≥ 3 receptors
≤ 2 receptors
B
****
****
****
D_{1-4} (µm²/s)
0.4
0.3
0.2
0.1
0.08
0.06
0.04
0.02
0.00
None
CXCL12
X4-gp120
D
****
****
****
MSI (a.u.)
15,000
10,000
5,000
4,000
3,000
2,000
1,000
0
None
CXCL12
X4-gp120

Figure 1

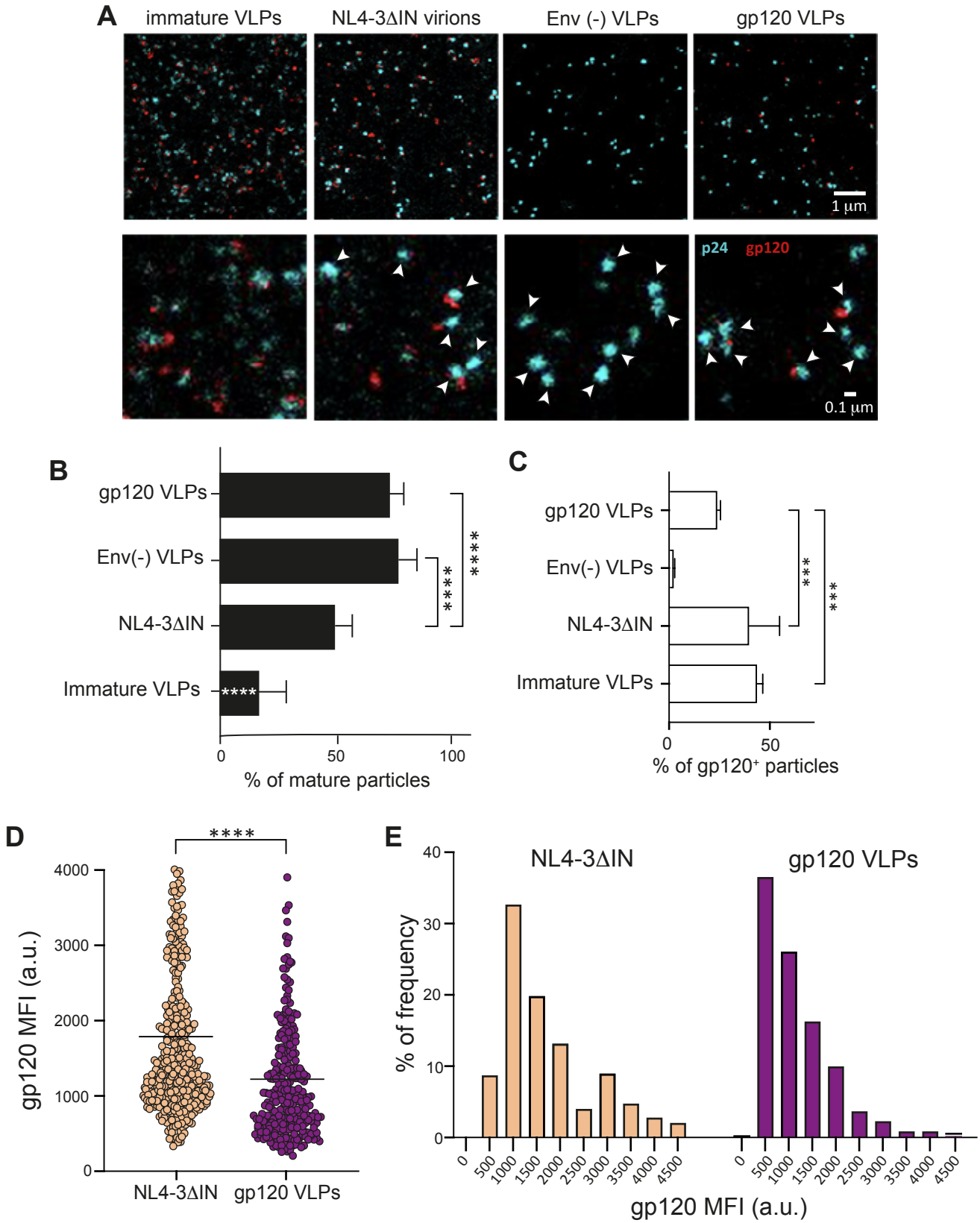
A
immature VLPs
NL4-3ΔIN virions
Env (-) VLPs
gp120 VLPs
1 µm
p24
gp120
0.1 µm
B
gp120 VLPs
Env(-) VLPs
NL4-3ΔIN
Immature VLPs
****
0
50
100
% of mature particles
C
gp120 VLPs
Env(-) VLPs
NL4-3ΔIN
Immature VLPs
***
0
50
% of gp120⁺ particles
D
****
gp120 MFI (a.u.)
4000
3000
2000
1000
0
NL4-3ΔIN
gp120 VLPs
E
NL4-3ΔIN
gp120 VLPs
% of frequency
40
30
20
10
0
0
500
1000
1500
2000
2500
3000
3500
4000
4500
gp120 MFI (a.u.)

Figure 2

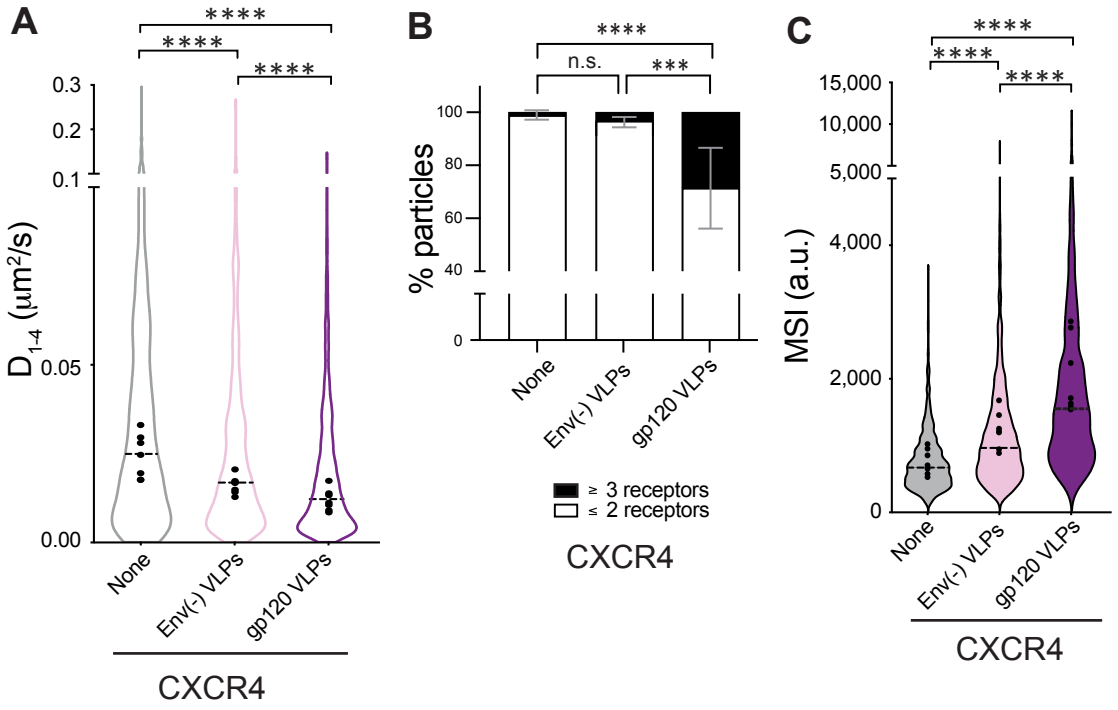
A
****
****
****
0.3
0.2
0.1
0.05
0.00
D1-4 (µm2/s)
None
Env(-) VLPs
gp120 VLPs
CXCR4
B
****
n.s.
***
100
80
60
40
0
% particles
None
Env(-) VLPs
gp120 VLPs
≥ 3 receptors
≤ 2 receptors
CXCR4
C
****
****
****
15,000
10,000
5,000
4,000
2,000
0
MSI (a.u.)
None
Env(-) VLPs
gp120 VLPs
CXCR4

Figure 3

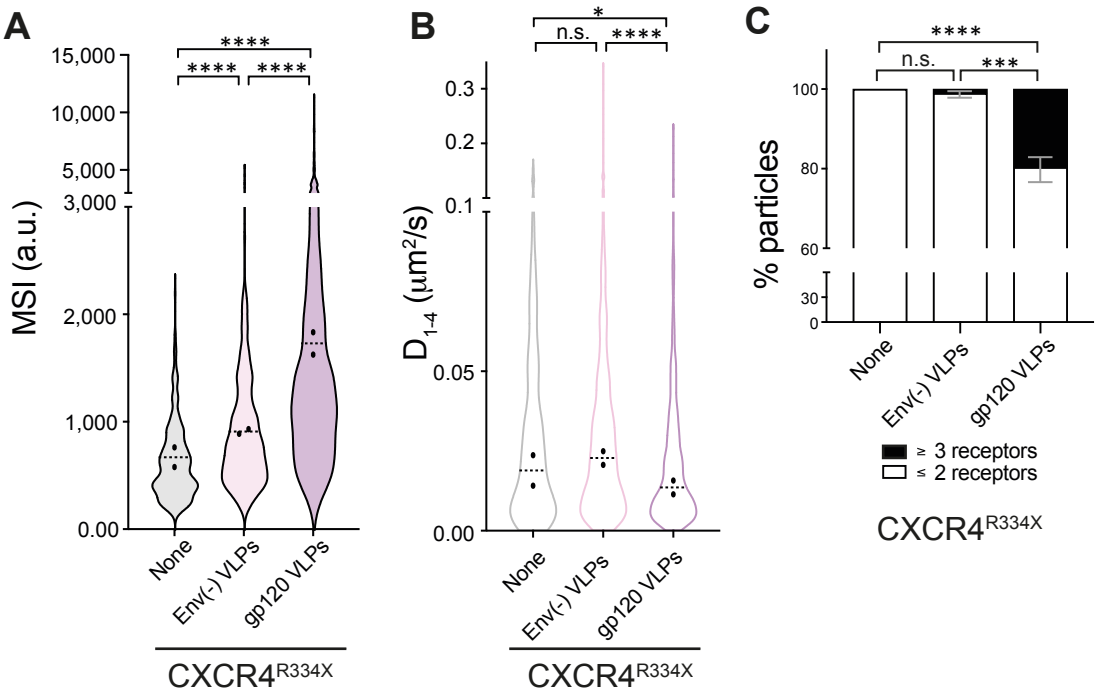
A
MSI (a.u.)
15,000
10,000
5,000
3,000
2,000
1,000
0.00
****
****
****
None
Env(-) VLPs
gp120 VLPs
CXCR4R334X
B
D1-4 (µm2/s)
0.3
0.2
0.1
0.05
0.00
*
n.s.
****
None
Env(-) VLPs
gp120 VLPs
CXCR4R334X
C
% particles
100
80
60
30
0
****
n.s.
***
None
Env(-) VLPs
gp120 VLPs
≥ 3 receptors
≤ 2 receptors
CXCR4R334X

Figure 4

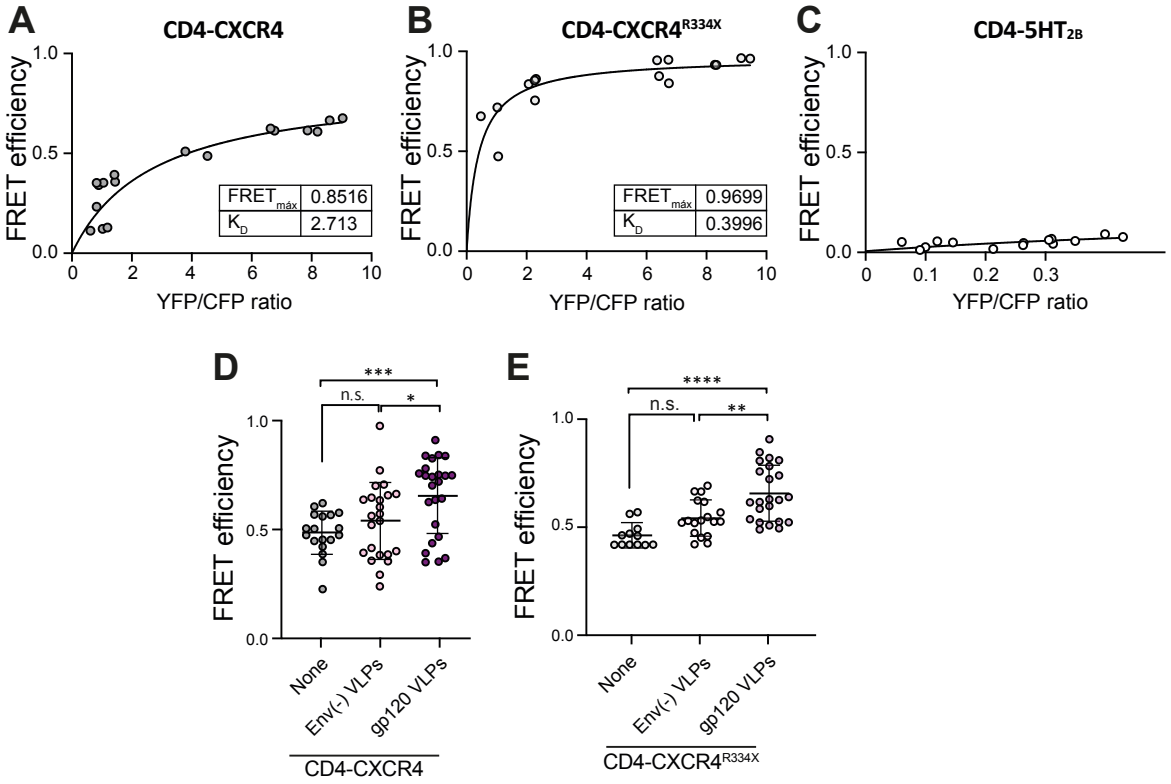
A
CD4-CXCR4
FRET efficiency
YFP/CFP ratio
FRETmáx 0.8516
KD 2.713
B
CD4-CXCR4R334X
FRET efficiency
YFP/CFP ratio
FRETmáx 0.9699
KD 0.3996
C
CD4-5HT2B
FRET efficiency
YFP/CFP ratio
D
FRET efficiency
***
n.s.
*
None
Env(-) VLPs
gp120 VLPs
CD4-CXCR4
E
FRET efficiency
****
n.s.
**
None
Env(-) VLPs
gp120 VLPs
CD4-CXCR4R334X

Figure 5

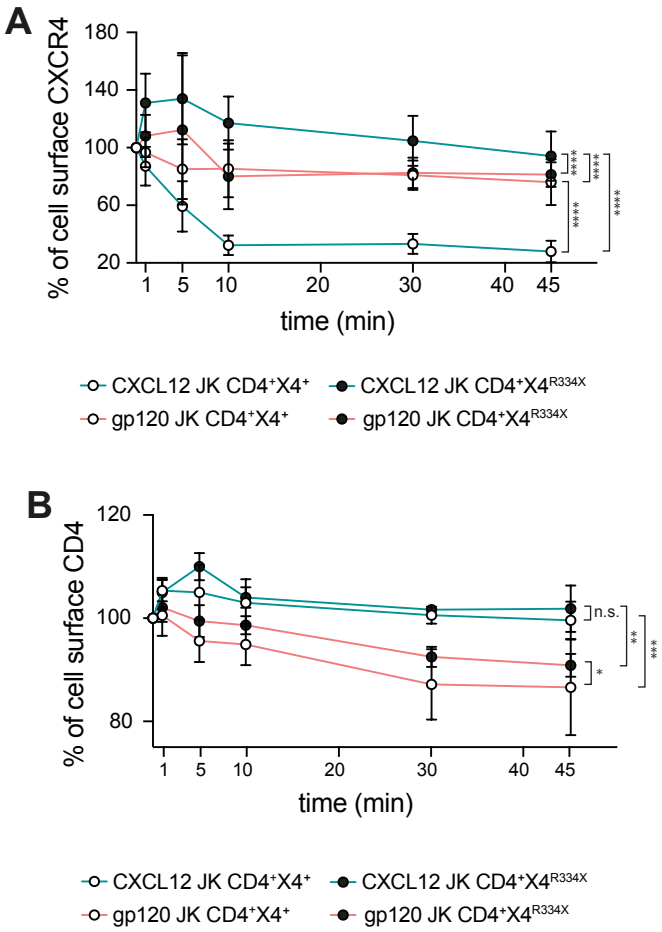
A
% of cell surface CXCR4
180
140
100
60
20
1
5
10
20
30
40
45
time (min)
****
****
****
****
CXCL12 JK CD4+X4+
CXCL12 JK CD4+X4R334X
gp120 JK CD4+X4+
gp120 JK CD4+X4R334X
B
% of cell surface CD4
120
100
80
1
5
10
20
30
40
45
time (min)
n.s.
**
***
*
CXCL12 JK CD4+X4+
CXCL12 JK CD4+X4R334X
gp120 JK CD4+X4+
gp120 JK CD4+X4R334X

Figure 6

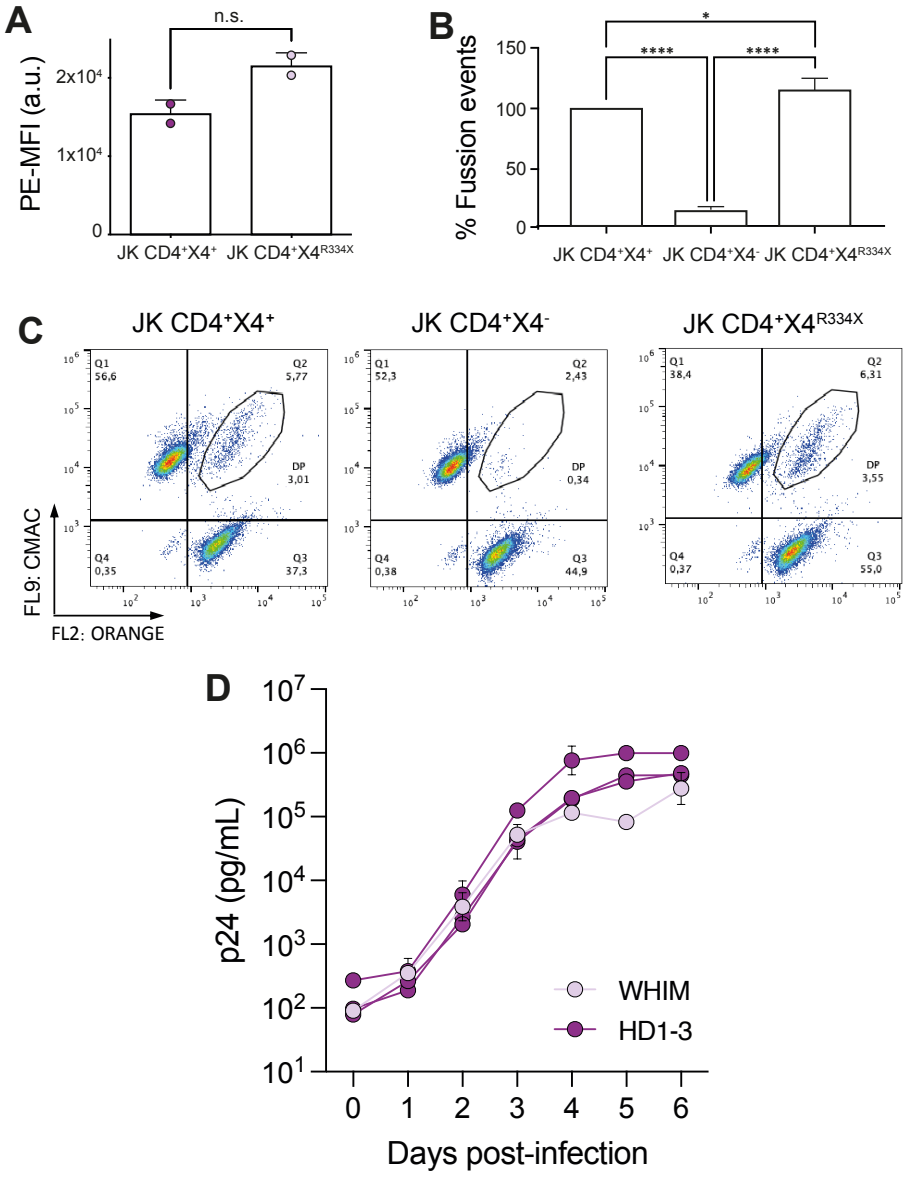
A
n.s.
PE-MFI (a.u.)
2x10⁴
1x10⁴
0
JK CD4⁺X4⁺
JK CD4⁺X4R334X
B
*
****
****
% Fussion events
150
100
50
0
JK CD4⁺X4⁺
JK CD4⁺X4⁻
JK CD4⁺X4R334X
C
JK CD4⁺X4⁺
JK CD4⁺X4⁻
JK CD4⁺X4R334X
Q1 56,6
Q2 5,77
DP 3,01
Q4 0,35
Q3 37,3
Q1 52,3
Q2 2,43
DP 0,34
Q4 0,38
Q3 44,9
Q1 38,4
Q2 6,31
DP 3,55
Q4 0,37
Q3 55,0
FL9: CMAC
FL2: ORANGE
D
p24 (pg/mL)
10⁷
10⁶
10⁵
10⁴
10³
10²
10¹
0
1
2
3
4
5
6
Days post-infection
WHIM
HD1-3

Figure 7